APPENDIX

APPENDIX A

Every energy profile for used in deterministic studies

Table A.1 Electricity load profile (Base load 2 MW)

Hour	Load (p.u.)	Hour	Load (p.u.)	Hour	Load (p.u.)
1	0.732	9	0.710	17	0.798
2	0.682	10	0.737	18	0.788
3	0.638	11	0.762	19	0.964
4	0.613	12	0.747	20	1
5	0.636	13	0.719	21	0.967
6	0.733	14	0.825	22	0.906
7	0.715	15	0.840	23	0.867
8	0.674	16	0.845	24	0.802

Table A.2 Heat load profile (Base load 2 MW)

Hour	Load (p.u.)	Hour	Load (p.u.)	Hour	Load (p.u.)
1	0.650	9	0.983	17	0.858
2	0.667	10	0.992	18	0.825
3	0.650	11	0.992	19	0.808
4	0.650	12	1	20	0.808
5	0.725	13	1	21	0.800
6	0.800	14	0.975	22	0.797
7	0.875	15	0.958	23	0.717
8	0.950	16	0.900	24	0.650

Table A.3 Solar power profile

Hour	Generation (kW)	Hour	Generation (kW)	Hour	Generation (kW)
1	0	9	484.224	17	369.615
2	0	10	696.251	18	137.531
3	0	11	868.164	19	5.730
4	0	12	999.965	20	0
5	0	13	999.965	21	0
6	0	14	939.795	22	0
7	34.383	15	787.938	23	0
8	243.544	16	598.833	24	0

Table A.4 Wind power profile

Hour	Generation (kW)	Hour	Generation (kW)	Hour	Generation (kW)
1	0	9	2000	17	469.543
2	109.424	10	2000	18	568.678
3	1860.538	11	852.158	19	0
4	2000	12	163.339	20	0
5	2000	13	121.572	21	31.561
6	2000	14	1103.843	22	36.961
7	2000	15	1131.437	23	109.425
8	2000	16	469.543	24	73.306

APPENDIX B

Hourly probabilistic scheduling results

(Graphical Data visualization)

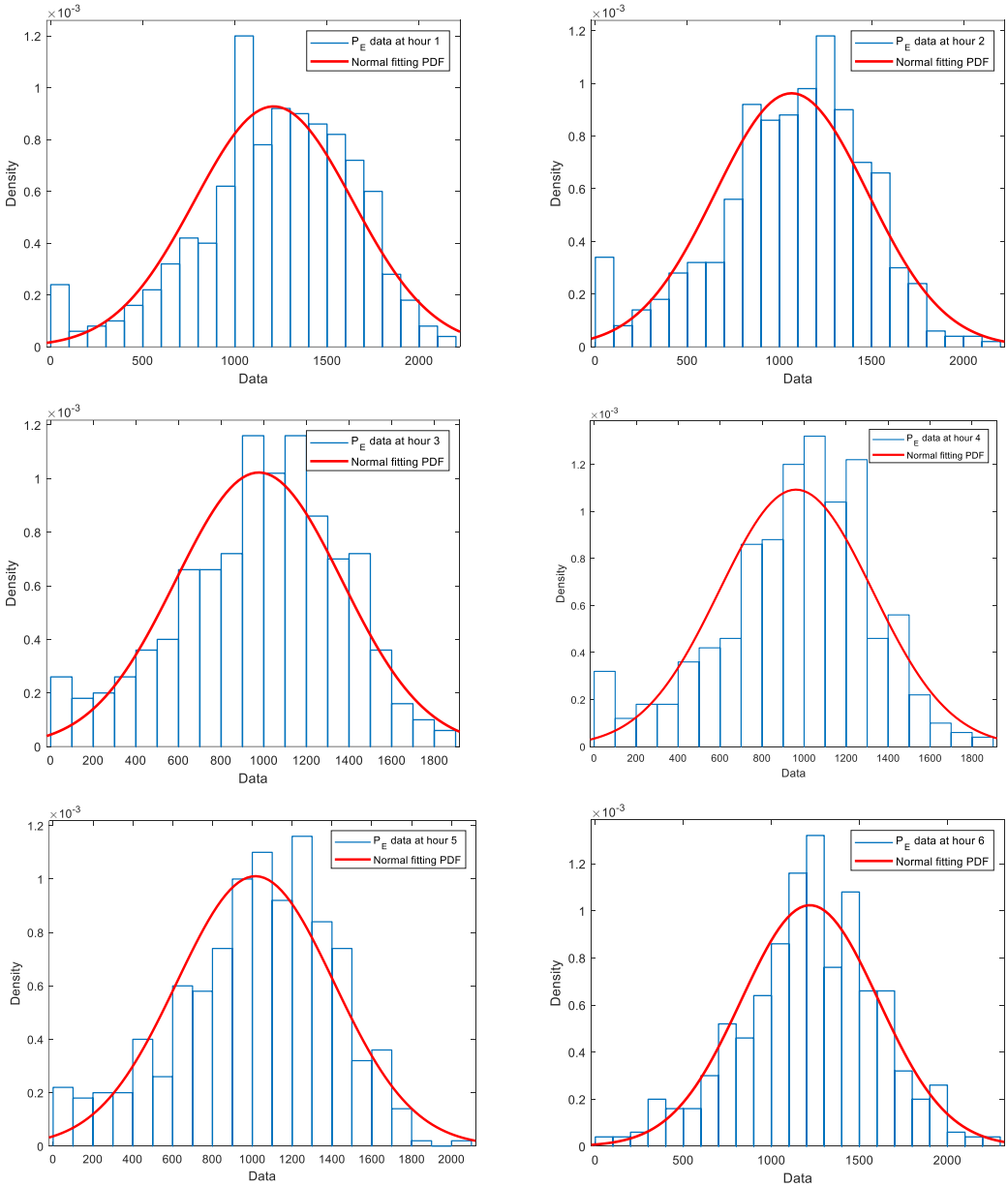

Figure B.1 The PDF of P_E scheduling in operating hours

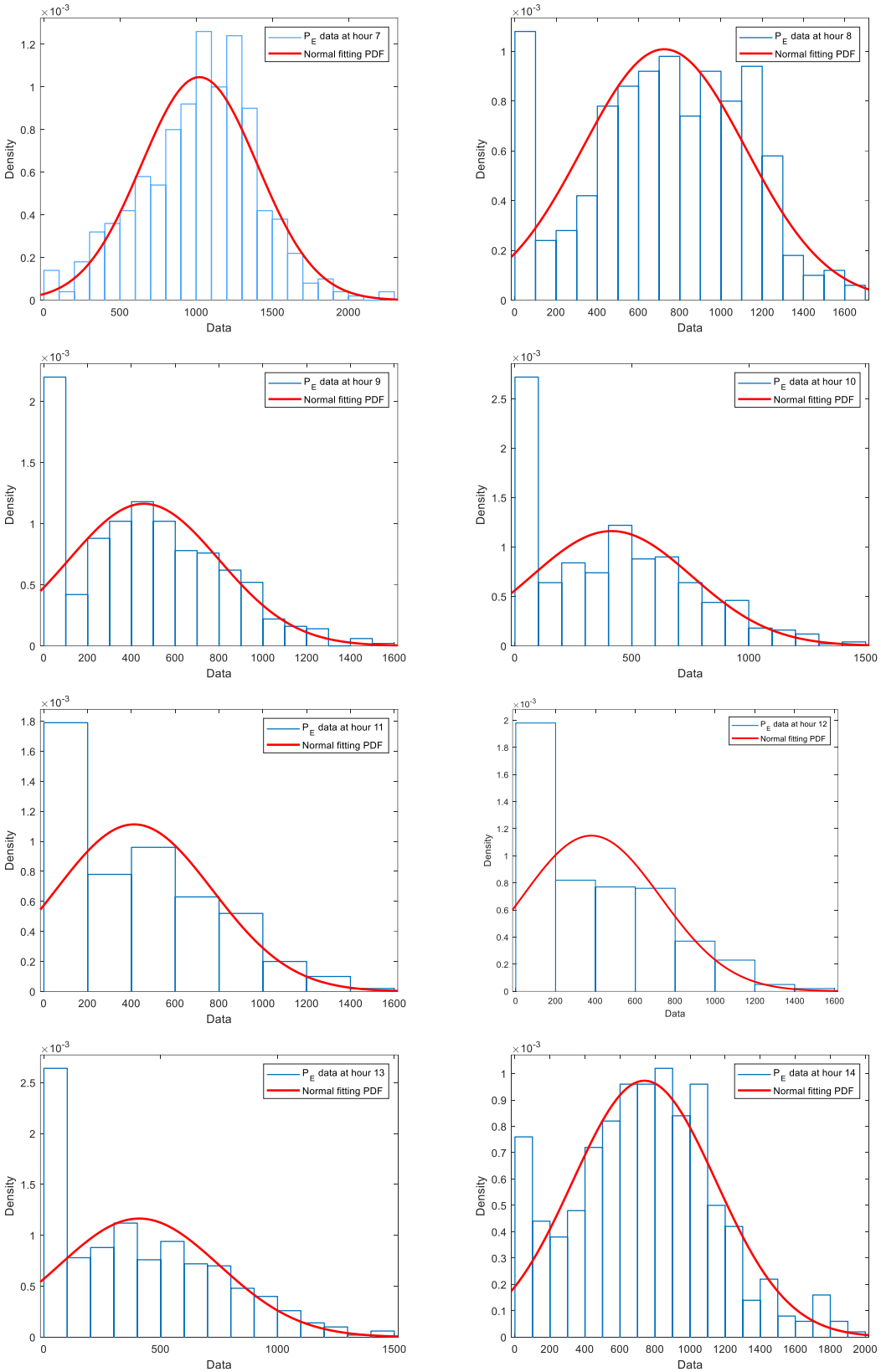

Figure B.1 The PDF of P_E scheduling in operating hours (Continued)

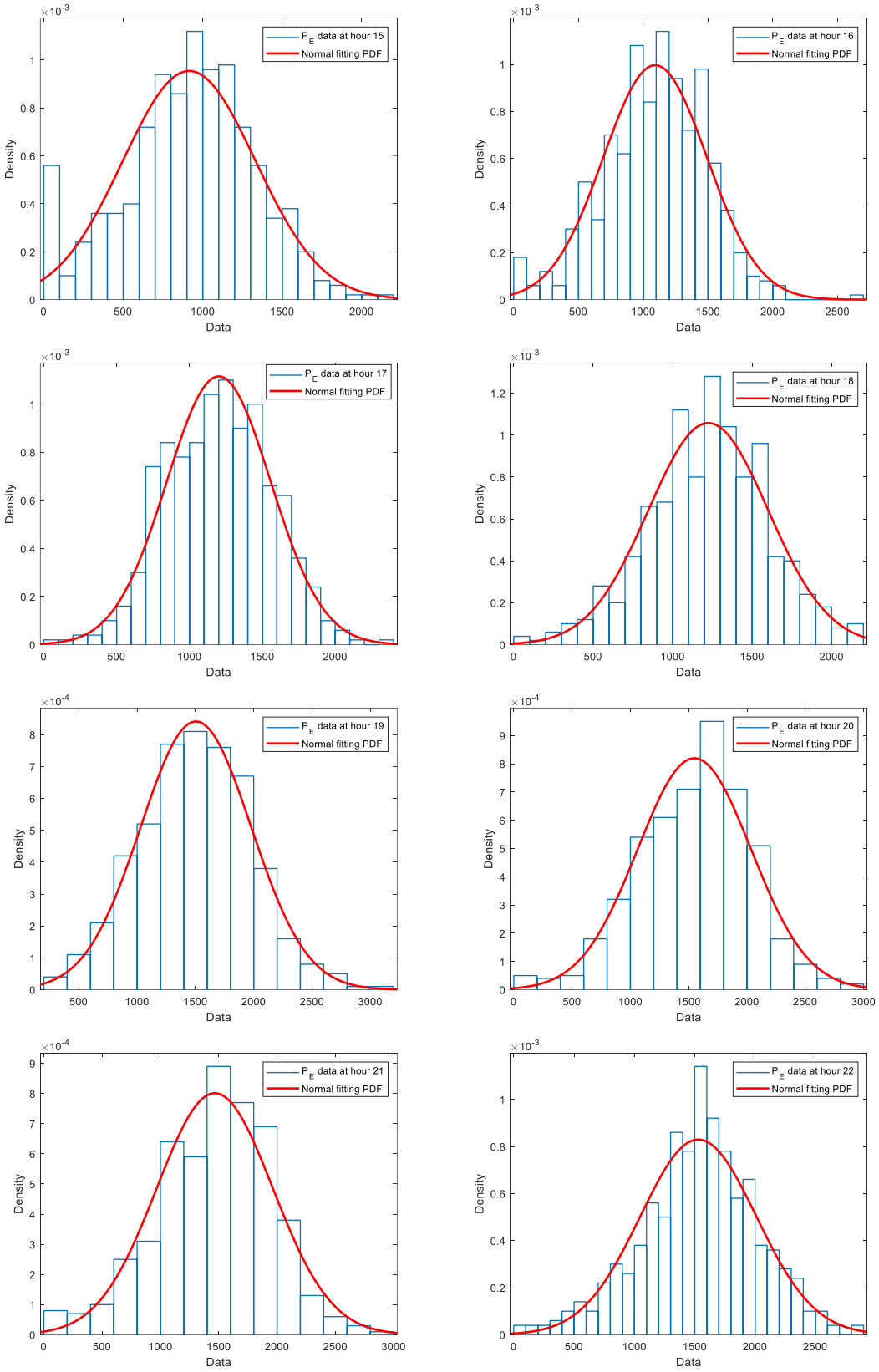

Figure B.1 The PDF of P_E scheduling in operating hours (Continued)

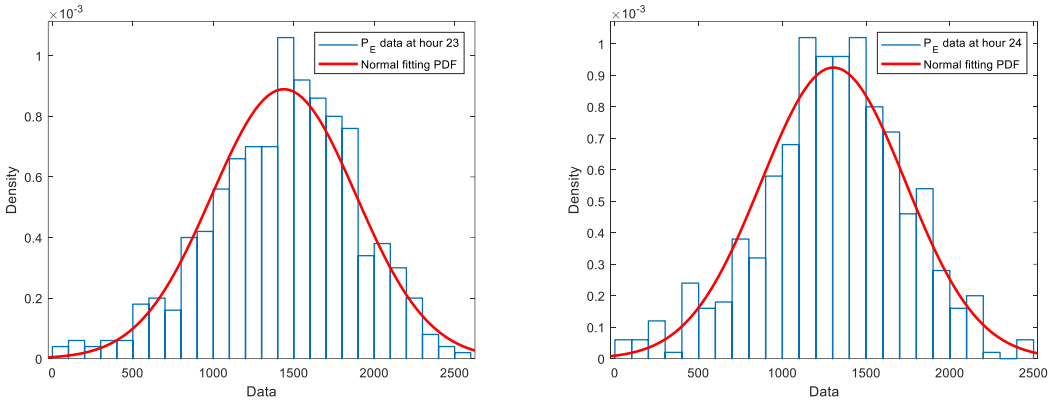

Figure B.1 The PDF of P_E scheduling in operating hours (Continued)

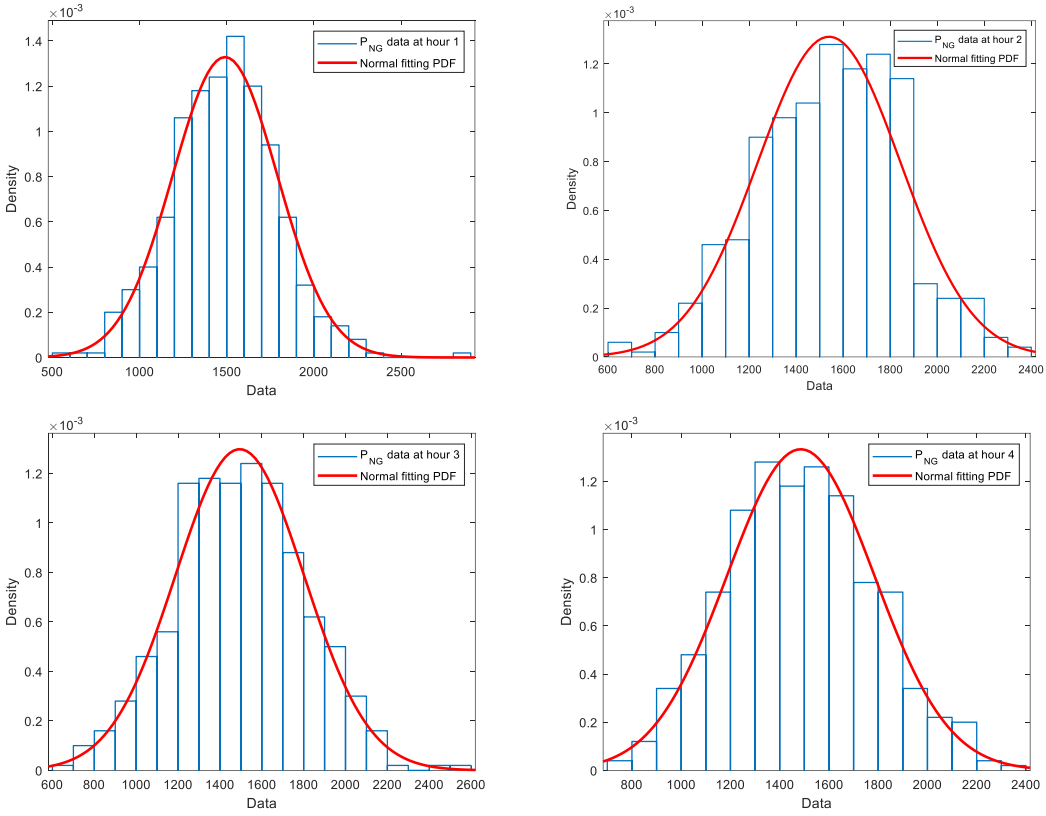

Figure B.2 The PDF of P_{NG} scheduling in operating hours

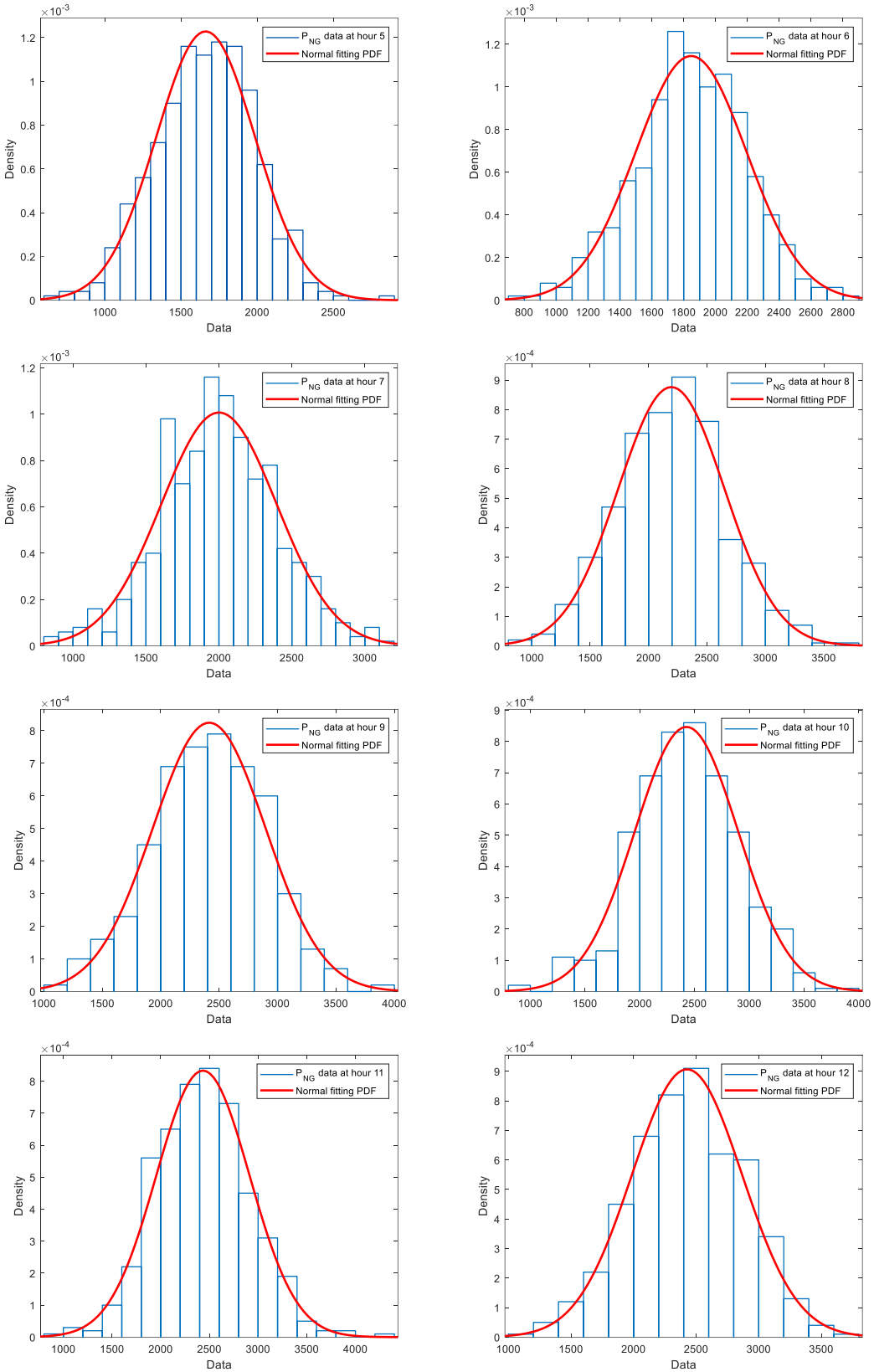

Figure B.2 The PDF of P_{NG} scheduling in operating hours (Continued)

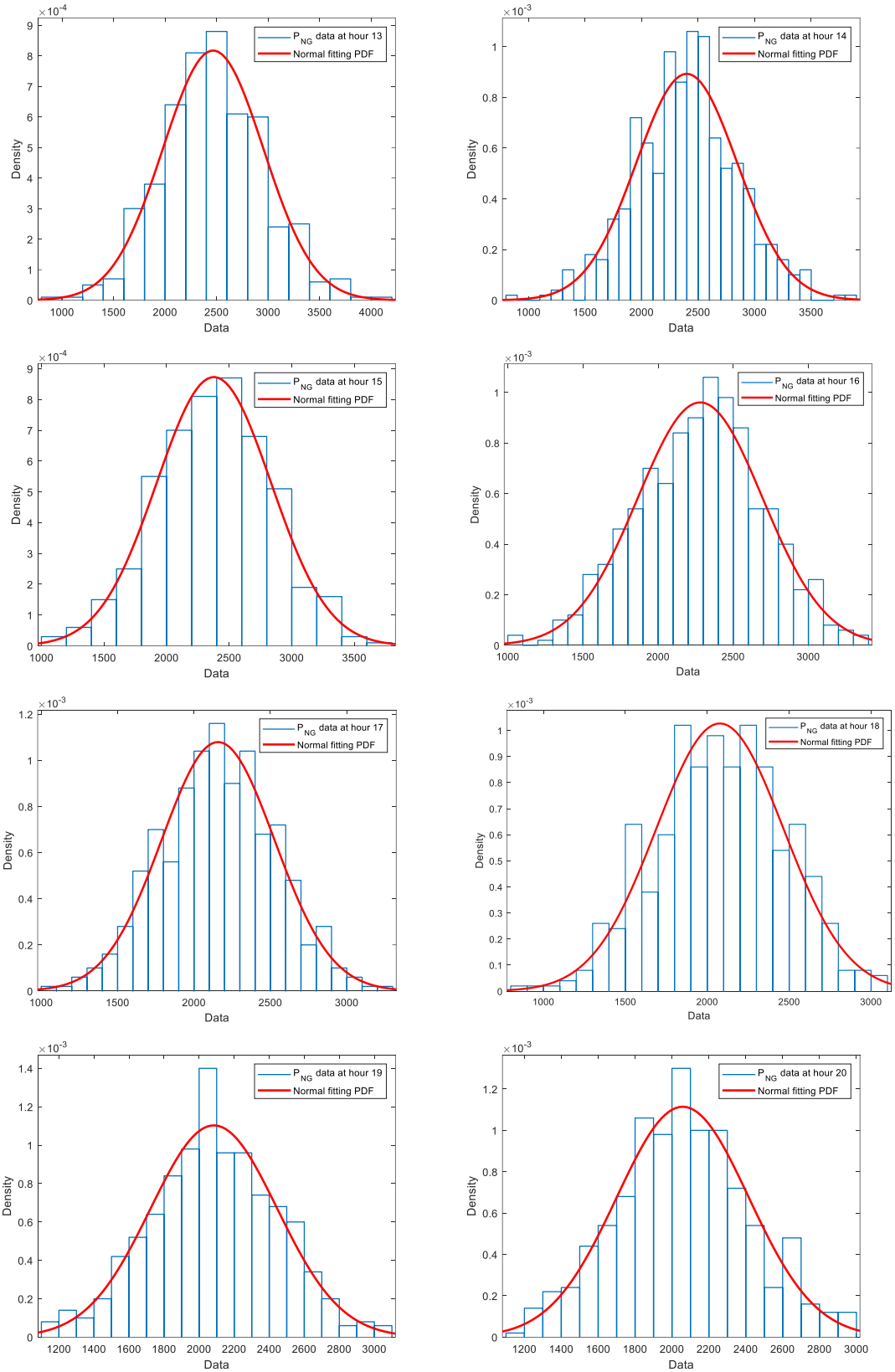

Figure B.2 The PDF of P_{NG} scheduling in operating hours (Continued)

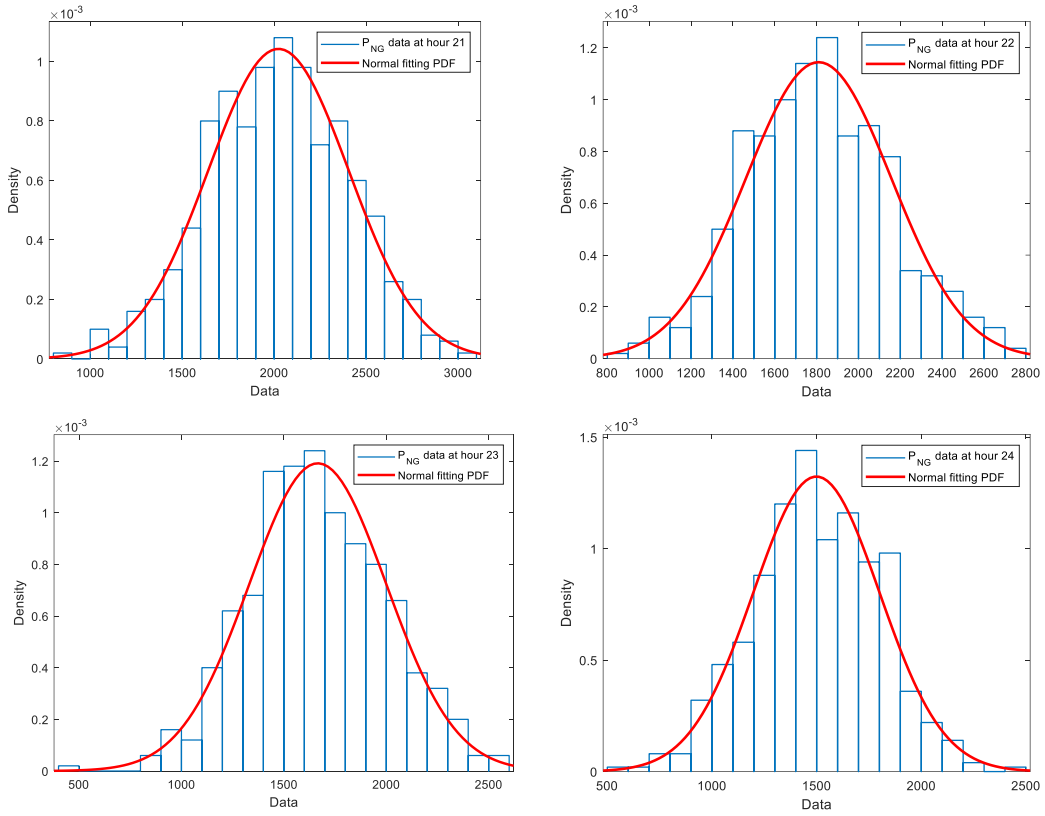

Figure B.2 The PDF of P_{NG} scheduling in operating hours (Continued)

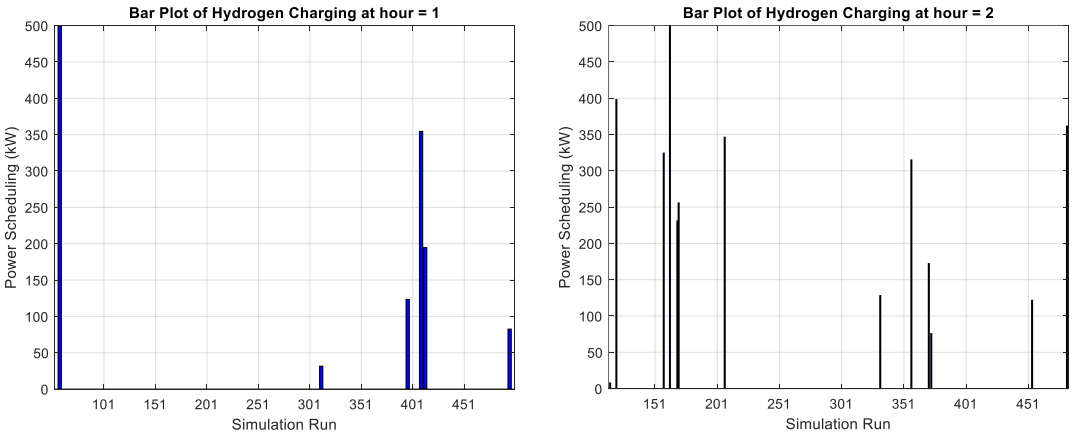

Figure B.3 The bar plot of P_{EL} which is hydrogen charging in operating hours

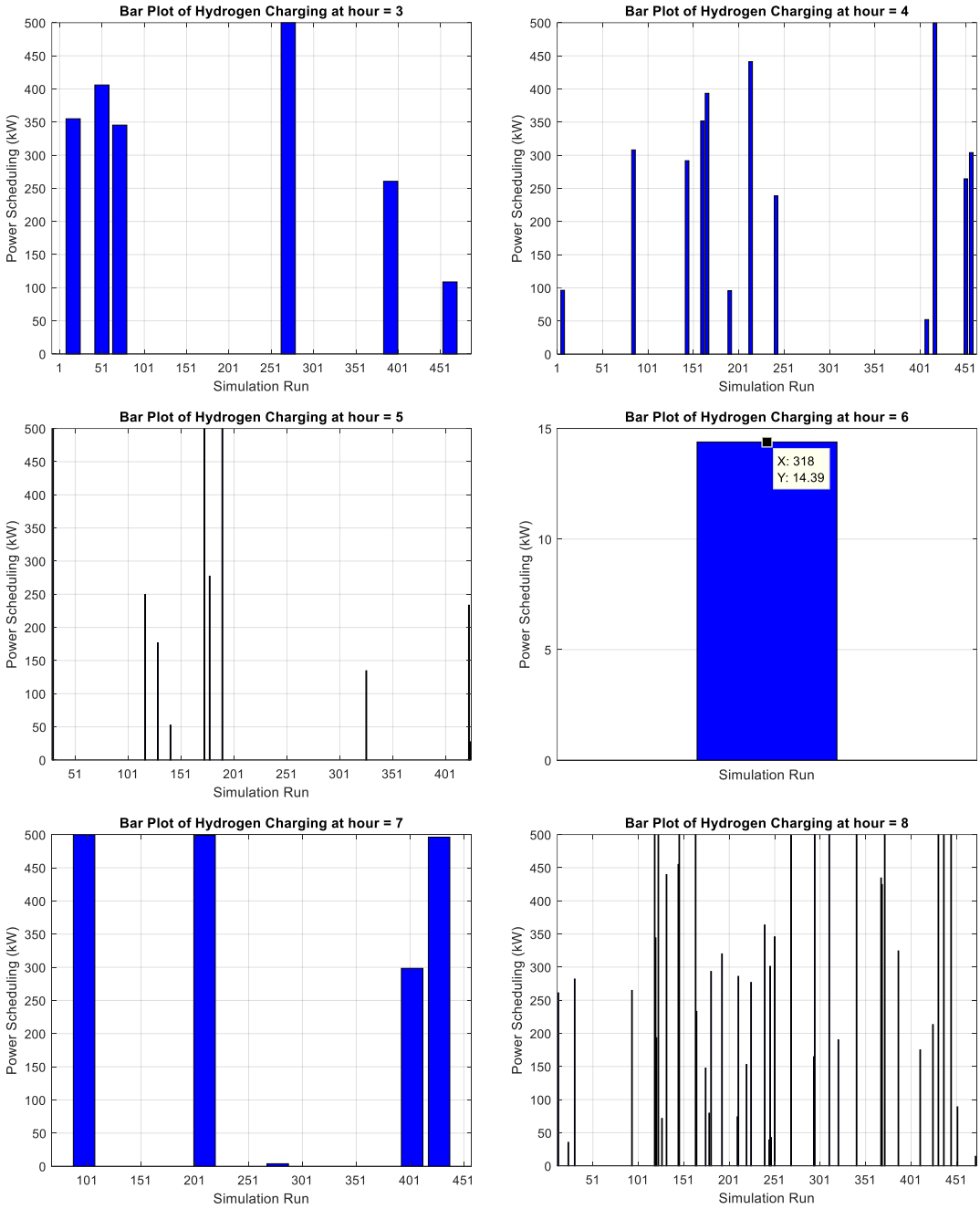

Figure B.3 The bar plot of P_{EL} which is hydrogen charging in operating hours (Continued)

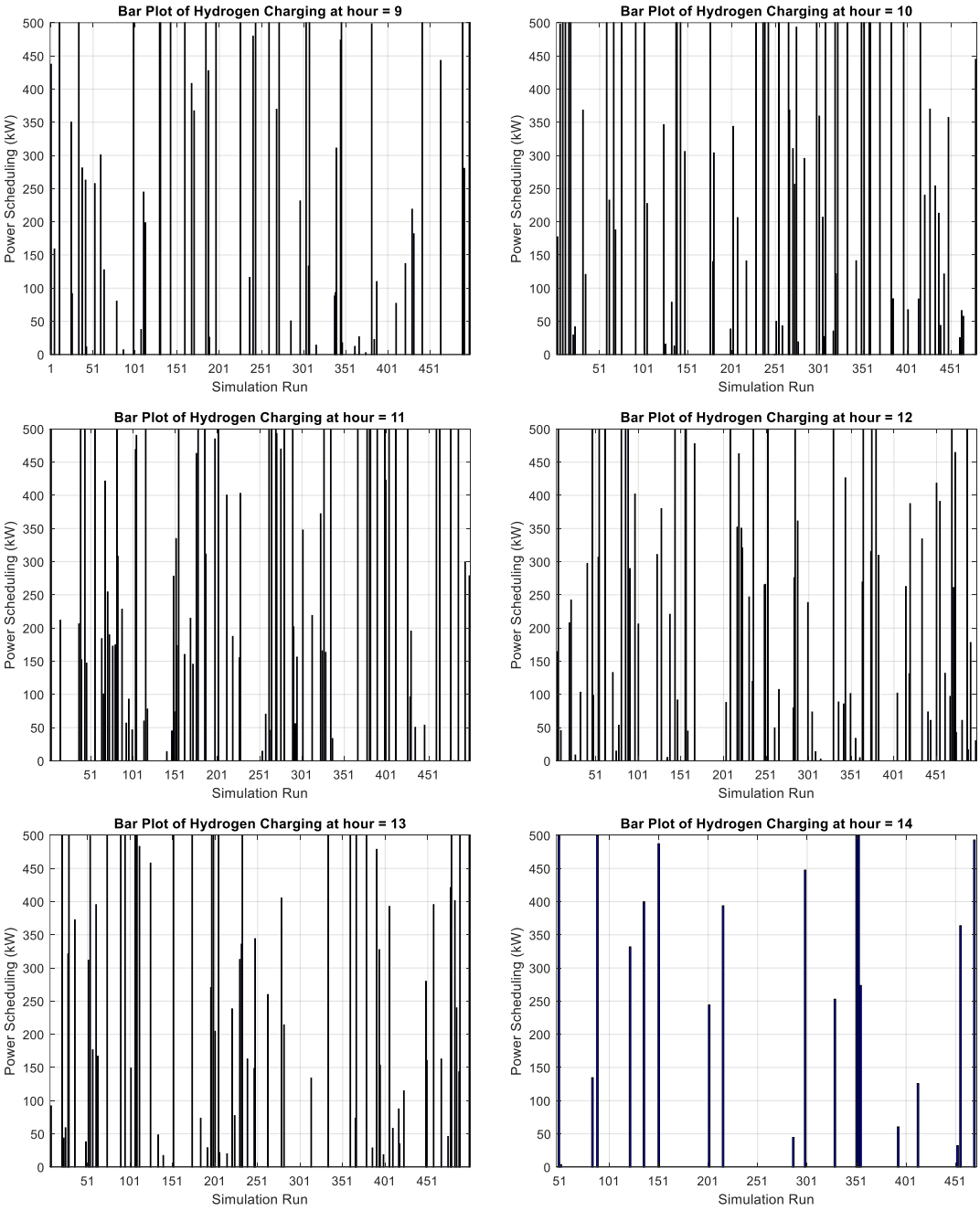

Figure B.3 The bar plot of P_{EL} which is hydrogen charging in operating hours (Continued)

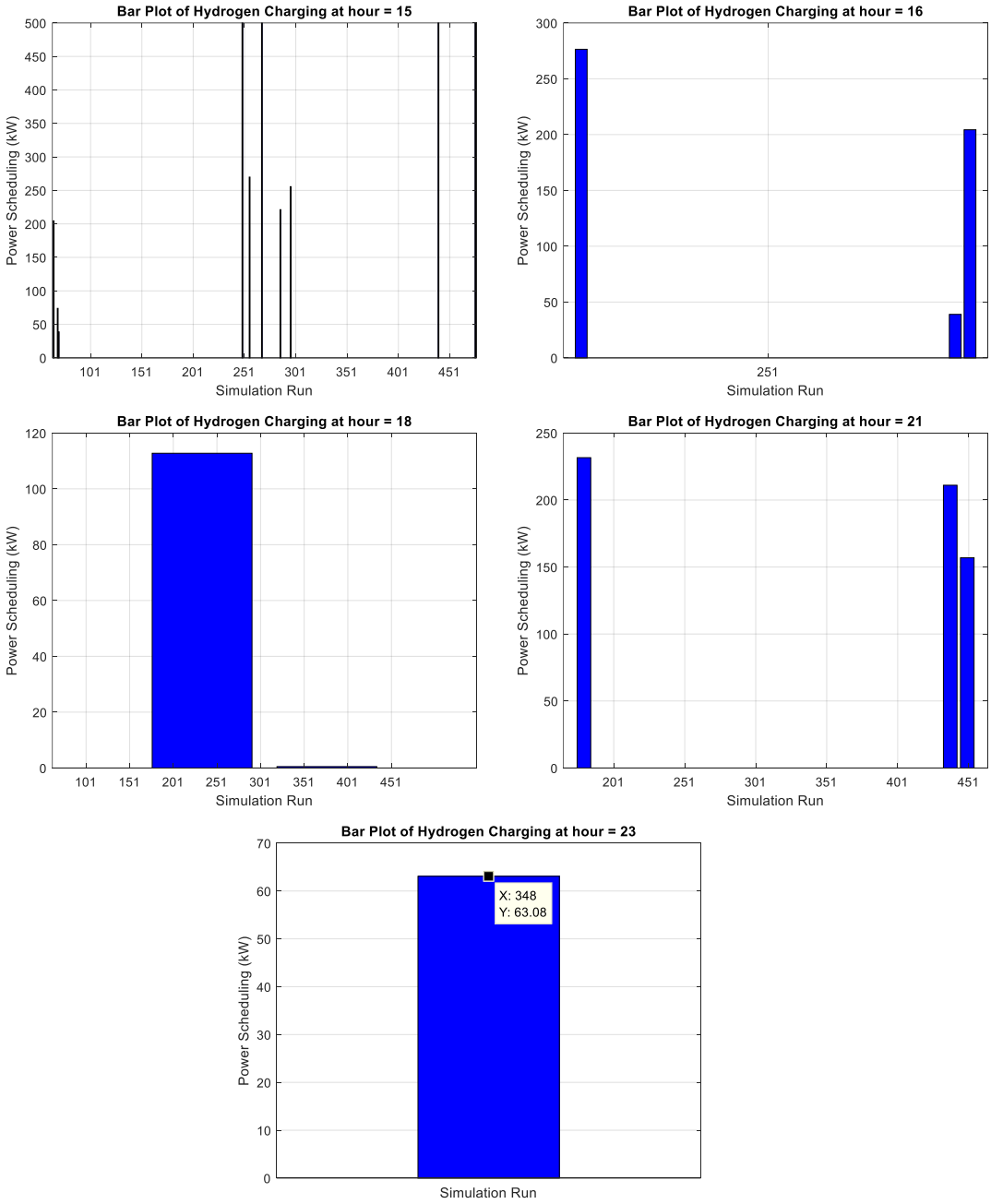

Figure B.3 The bar plot of P_{EL} which is hydrogen charging in operating hours (Continued)

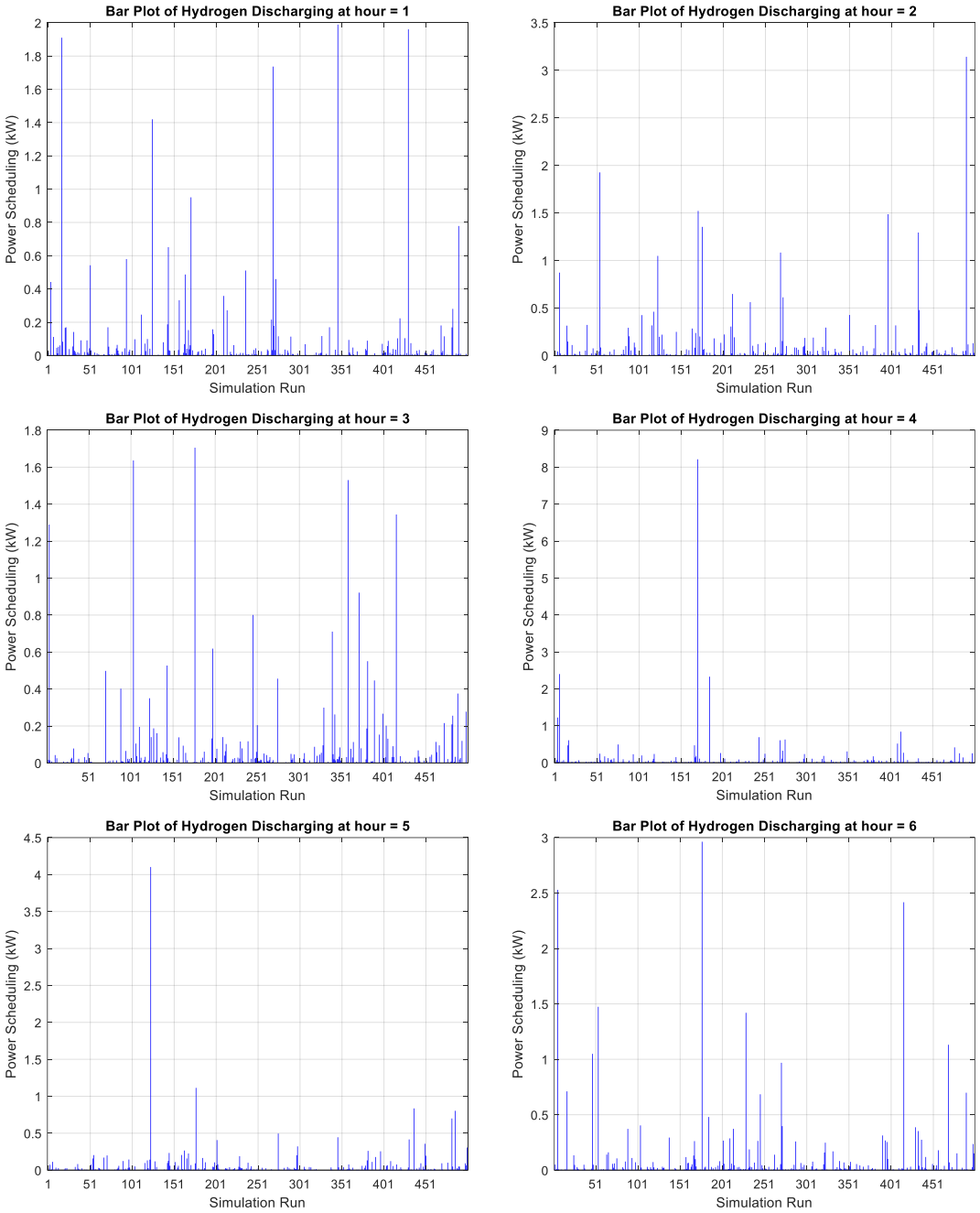

Figure B.4 The bar plot of P_{FC} which is hydrogen discharging in operating hours

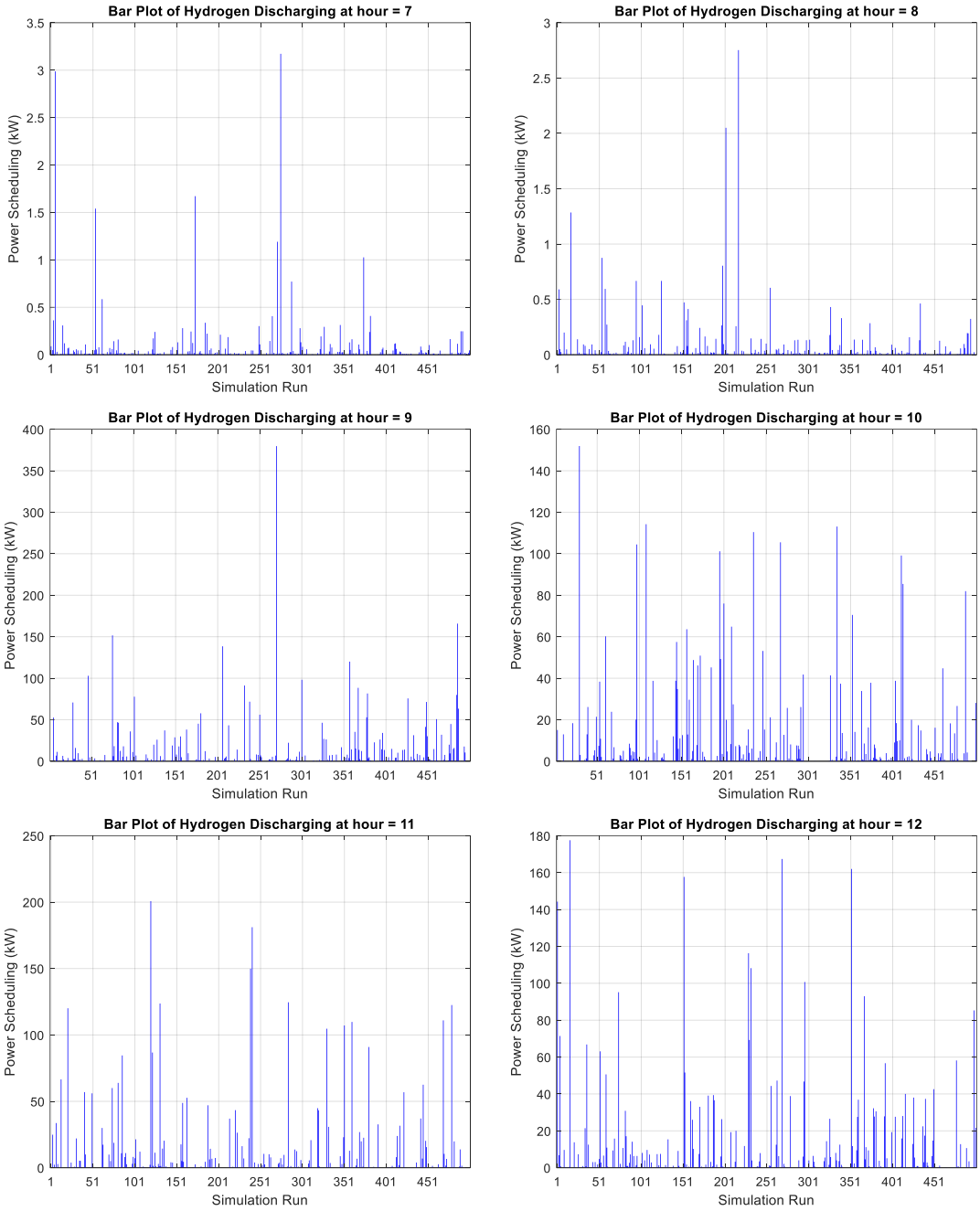

Figure B.4 The bar plot of P_{FC} which is hydrogen discharging in operating hours (Continued)

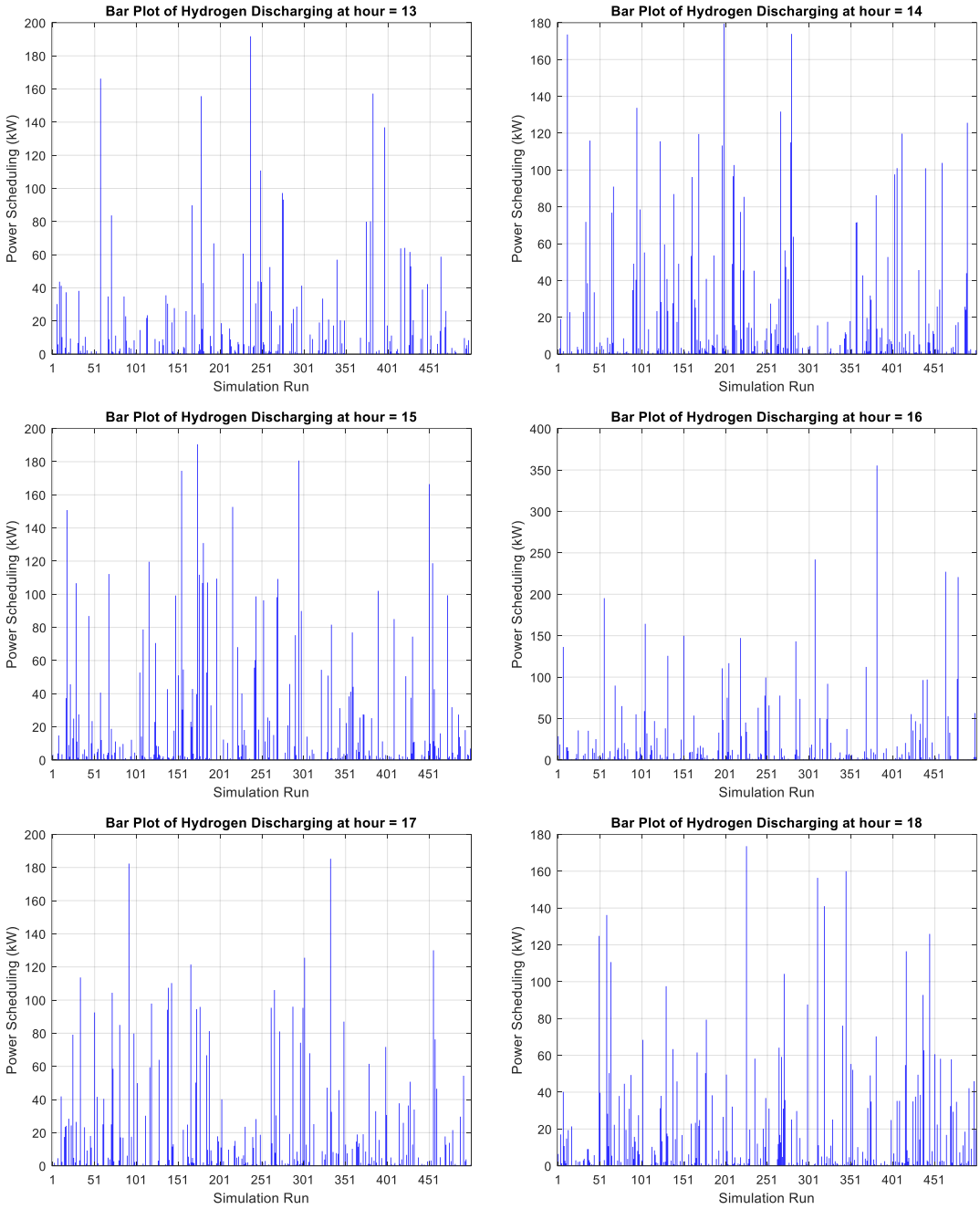

Figure B.4 The bar plot of P_{FC} which is hydrogen discharging in operating hours (Continued)

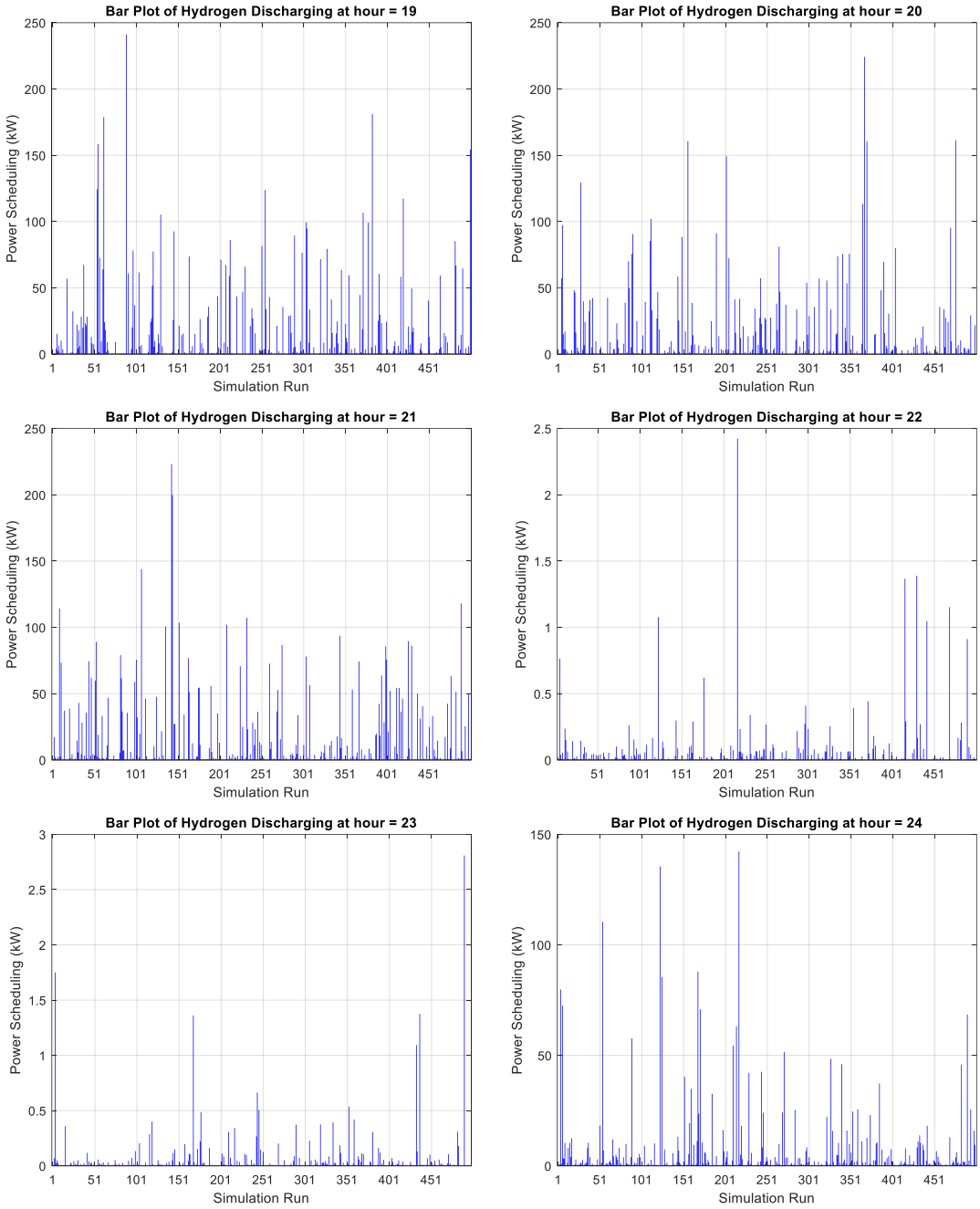

Figure B.4 The bar plot of P_{FC} which is hydrogen discharging in operating hours (Continued)

APPENDIX C

Detailed Simulation Results for Varying Initial Pressure in Case V under TOU Tariffs Considerations

This appendix presents the simulation results for various initial pressure values tested under OMES-WSPHS model with TOU tariffs in Case V. The results provide insights into how different initial pressure values impact system performance, as objective function in TOC. The data are organized as follows:

Table C.1 Simulation results for 40 bar Initial pressure

Energy scheduling	Energy (kWh)	Costs	TOC
Electricity	13,698.62	51,399.14	240,717.78
NG	47,329.66	189,318.64	
HS	6,531.35	-	

Table C.2 Simulation results for 60 bar Initial pressure

Energy scheduling	Energy (kWh)	Costs	TOC
Electricity	13,697.84	52,543.83	241,862.47
NG	47,329.66	189,318.64	
HS	6,533.94	-	

Table C.3 Simulation results for 80 bar Initial pressure

Energy scheduling	Energy (kWh)	Costs	TOC
Electricity	14,019.32	54,880.09	244,113.58
NG	47,308.37	189,233.49	
HS	5,535.44	-	

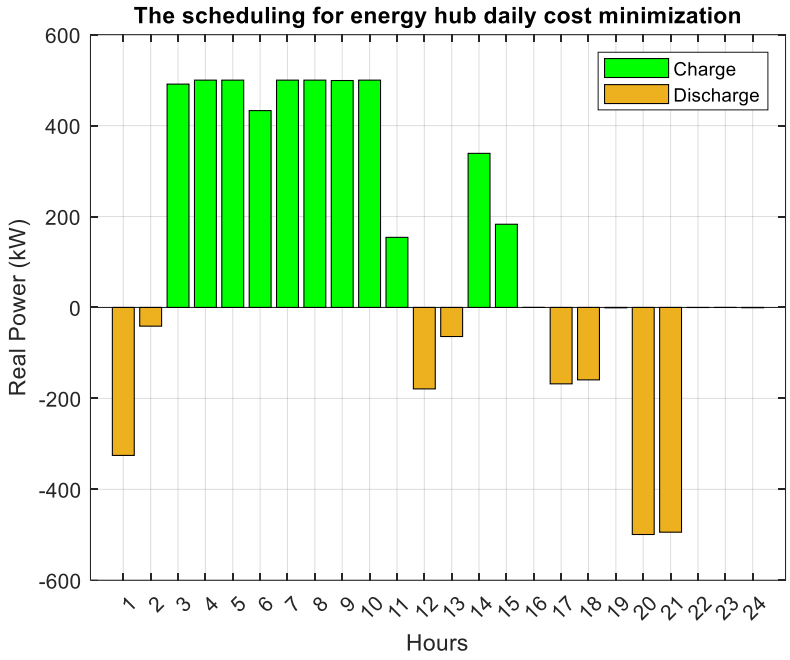

(a)

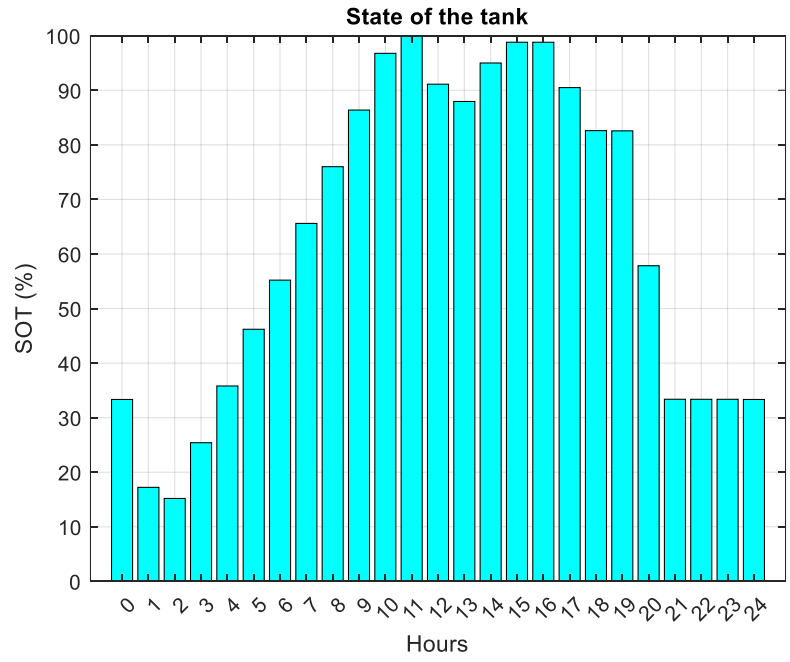

(b)

Figure C.1 (a) HS scheduling for 24 hours and (b) SOT 40 bar Initial pressure

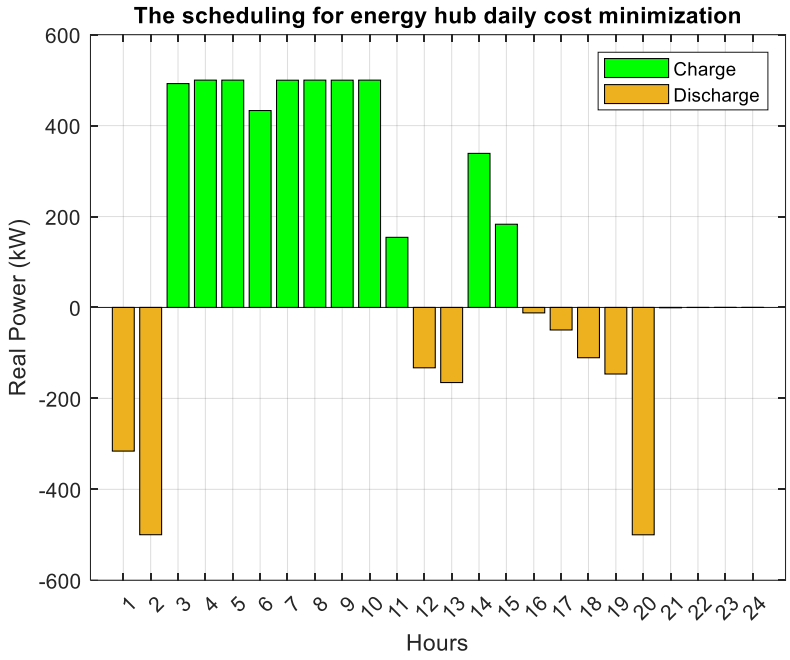

(a)

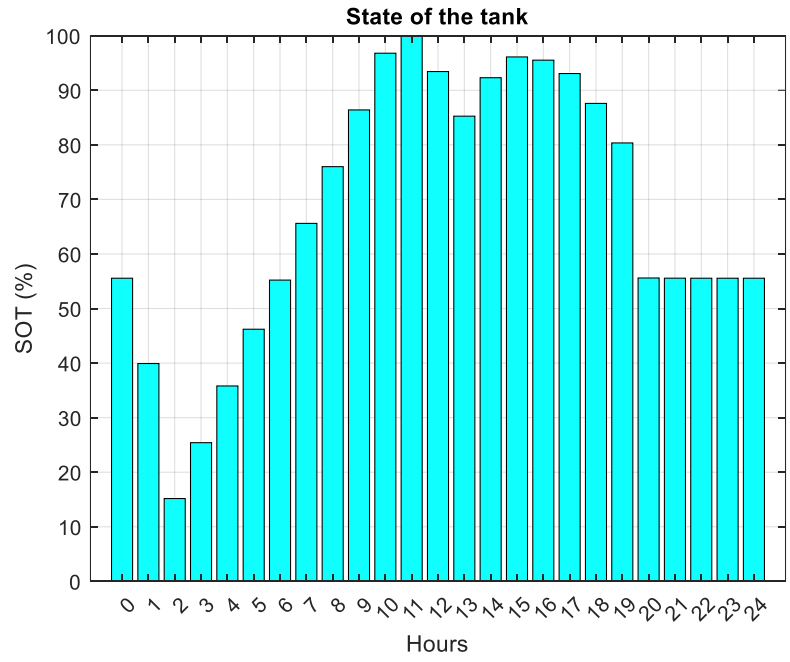

(b)

Figure C.2 (a) HS scheduling for 24 hours and (b) SOT for 60 bar Initial pressure

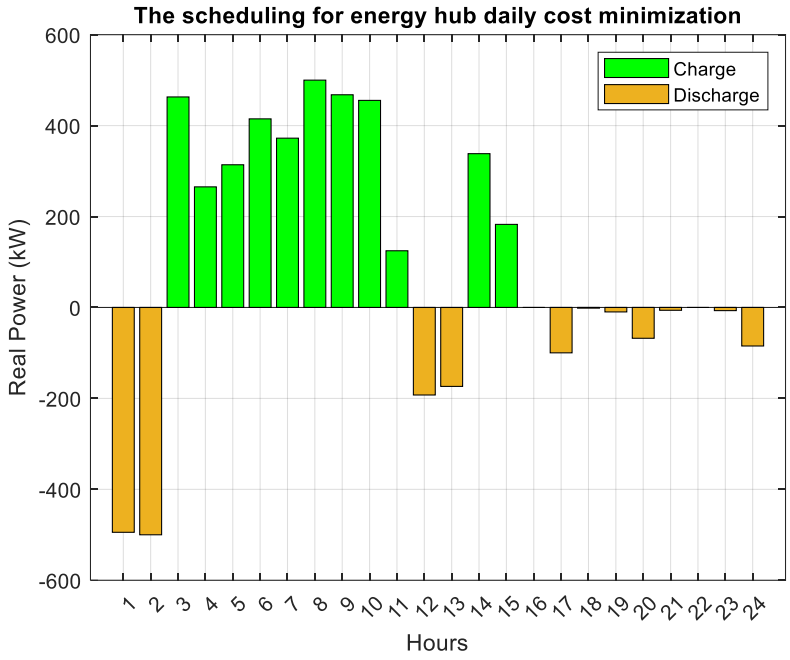

(a)

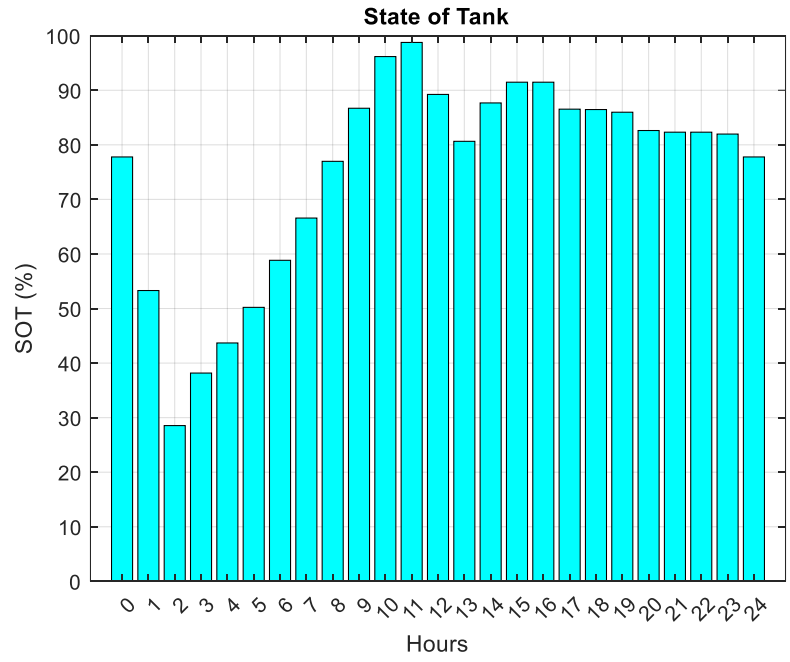

(b)

Figure C.3 (a) HS scheduling for 24 hours and (b) SOT for 80 bar Initial pressure

APPENDIX D

List of publications

S. Dechjinda and K. Chayakulkheeree (2024), Optimal Daily Scheduling of Hybrid Wind-Hydrogen Storage using Particle Swarm Optimization, 2024 International Electrical Engineering Congress (iEECON2024), Pattaya, Thailand.

S. Dechjinda and K. Chayakulkheeree (2024), Optimal scheduling of multi-energy systems with wind-solar power and hydrogen storage integration., GMSARN International Journal.

2024 International Electrical Engineering Congress (iEECON 2024)
March 6-8, 2024, Pattaya Chonburi, THAILAND

Optimal Daily Scheduling of Hybrid Wind-Hydrogen Storage Using Particle Swarm Optimization

Suttipong Dechjinda **Keerati Chayakulkheeree**

School of Electrical Engineering
Institute of Engineering, Suranaree University of Technology
Nakhonratchasima, Thailand
E-mail: suttipong.dechjinda@gmail.com, keerati.ch@sut.ac.th

***Abstract*— This paper proposes a particle swarm optimization-based optimal daily scheduling (PSO-ODS) for hybrid wind-hydrogen storage (HWHS). Minimizing daily energy loss (DL) is the main goal of the presented method. The approaches of PSO-ODS for HWHS were inspected with the modified IEEE 33-bus system with HWHS integration using load and wind profiles of Thailand. The studies are separated into two cases, which are the wind-integrated system with and without hydrogen storage optimal scheduling. The proposed approach can effectively decrease DL for the HWHS integrated distribution system, as indicated by the simulation results.**

Keywords— optimal daily scheduling, hydrogen storage, particle swarm optimization, wind energy.

NOMENCLATURE

ch	:	The matrix of charging of hydrogen storage.
dch	:	The matrix of discharging of hydrogen storage.
NB	:	The total number of buses.
NT	:	The total number of wind turbines.
PN	:	The penalty functions.
P_{EL}	:	The power of electrolyzer (kW).
$P_{EL,rated}$	:	The rated power of electrolyzer (kW).
P_{FC}	:	The power of fuel cell (kW).
$P_{FC,rated}$	:	The rated power of fuel cell (kW).
η_{EL}	:	The efficiency of electrolyzer (%).
η_{FC}	:	The efficiency of fuel cell (%).
E_{tank}	:	The energy of the hydrogen tank (kWh).
$E_{tank,rated}$	:	The rated energy of the hydrogen tank (kWh).
$P_{loss,h}$	:	The hourly power loss (kW).
DL	:	The daily energy loss (kWh).
$P_{w,h}$	:	The hourly wind power output (kW).
$P_{w,rated}$	:	The rated wind turbine (kW).
$P_{wpp,h}$	:	The hourly power output of wind power plants (kW).
V_i	:	The voltage of bus i (p.u.).
v_h	:	The wind velocity per hour (m/s).
$v_{w,rated}$	:	The rated wind velocity (m/s).
$v_{cut\text{-}in}$	:	The wind velocity specification allows the wind turbine to generate power (m/s).
$v_{cut\text{-}off}$	:	The wind speed specification allows the wind turbine to halt generating power (m/s).
G_{ij}	:	The line's conductance across buses i and j for $i \neq j$ (S).
δ_i	:	The angle bus voltage i (radian).

I. INTRODUCTION

Nowadays, energy from renewable sources is facing a significant challenge due to its inherent instability. The discontinuous pattern of renewable resources is one of their primary drawbacks, with most sources being unavailable for consistent utilization. For instance, wind power experiences fluctuations in wind speed, leading to unpredictable energy generation [1]. Although wind energy presently has the most developed technology, the most favorable large-scale improvement circumstances, and the most promising commercial growth tendency among renewable energy sources, its instability and unpredictability provide significant challenges to the power grid's ability to operate safely and steadily. A significant amount of wind energy is wasted when it is required to give up the wind in order to protect the power system, particularly when peak shaving is challenging [2]. Consequently, the significance of implementing energy storage systems grows as the amount of power produced from renewable resources rises [1-2]. There are several approaches to storing energy. One of the most modern technologies for storing surplus energy generated during off-peak hours is the retention of hydrogen. that has been stored can then be used to generate energy at peak times [3].

Hydrogen energy storage system (HESS) is a potential option for decarbonizing energy systems since it can produce electricity by using carbon-neutral renewable energy resources. When employed as an energy source, hydrogen exhibits the advantage of emitting no CO_2, making it an environmentally friendly alternative. Therefore, hydrogen energy storage is suitable for storing secondary energy. However, the challenge with hydrogen production from renewable sources is the low overall efficiency of energy conversion results in considerable energy and monetary losses [4-5].

As a result, much research related to hybrid wind-hydrogen system (HWHS) scheduling has been proposed. Hong et al. [2] investigated the optimal scheduling approach for the HWHS system while taking wind power efficiency into consideration. The artificial bee colony technique was utilized to tackle the problem of hydrogen production, increasing efficiency by 4.8%. O. Utomo et al. [4] discussed the optimal effective operations of a hydrogen storage and a fuel cell-connected energy system. The energy hub approach describes the system's mathematical structure. Meanwhile, linear programming is employed to lower total operating costs.

979-8-3503-8359-1/24/$31.00 ©2024 IEEE

2024 International Electrical Engineering Congress (iEECON 2024)
March 6-8, 2024, Pattaya Chonburi, THAILAND

G. He et al. [5] proposed an improved particle swarm optimization algorithm (IDW-PSO) that uses dynamic inertia weight adjustment to optimize the capacity configuration of a wind-solar hydrogen storage microgrid system. The approach improves optimization accuracy, lowers the probability of falling into the optimal location, and increases iteration performance.

There is plenty of knowledge and development needed for HWHS integration. Therefore, this paper proposes optimal daily scheduling (ODS) of HWHS to minimize daily energy loss (*DL*). The particle swarm optimization (PSO) is used to solve the proposed ODS for HWHS. To ascertain the validity and efficiency of the proposed approach, the modified IEEE 33-bus test system with HWHS is used as a case study.

The paper is structured in the following format. Section II addresses the HWHS modeling. The PSO-based ODS algorithm for resolving HWHS is presented in Section III. Section IV demonstrates and discusses the simulation results of the proposed PSO-ODS for HWHS using the modified IEEE 33-bus system. Finally, Section V provides the conclusion.

II. HWHS Modeling

For HWHS modeling, the wind power plant (WPP) and HESS are connected to a bus. While WPP generates the electricity, HESS schedules to eliminate wind power curtailment and regulate the power fluctuations. The model of the distribution system with HWHS is shown in Fig.1.

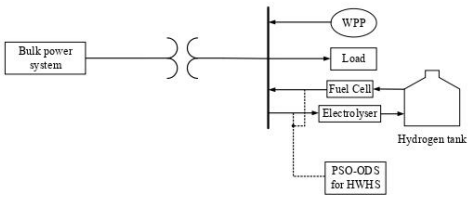

Fig. 1. The model of distribution system with HWHS.

A. Wind Power Modeling

A wind turbine will produce power when its velocity comes between the turbine's rated speed and the cut-in speed. If the velocity of the wind rises above the turbine's rated speed but falls below the cut-off speed, the output keeps the rated power constant. When the velocity of the wind surpasses the cut-off speed, the turbine is either halted to prevent the blades from rotating or pitched out of the wind.

A representation of the power performed from a wind turbine is (1) [6]:

$$P_{w,h}=\begin{cases} 0 \quad \text{for} \quad 0<v_h\le v_{cut-in}, \\ P_{w,rated}\times\left(\dfrac{v_h}{v_{w,rated}}\right)^3 \ \text{for} \ v_{cut-in}<v_h\le v_{w,rated}, \\ P_{w,rated} \quad \text{for} \quad v_{w,rated}<v_h\le v_{cut-off}, \\ 0 \quad \text{for} \quad v_h>v_{cut-off}. \end{cases} \tag{1}$$

The real power is injected into the load bus for peak shaving, whereas oscillation in wind speed affects the ability to cut peak during high demand times.

WPP consists of many wind turbines installed; the wind power of wind turbines in each hour is calculated from (1). When calculating the sum of wind power from all wind turbines, it is formulated as (2),

$$P_{wpp,h}=\sum_{i=1}^{NT}P_{w,i,h}. \tag{2}$$

B. HESS Modeling

Typically, the HESS consists of a pressurized gas tank, an electrolyzer, and fuel cells. The electrolyzer transforms electricity into a chemical substance in the shape of hydrogen when there is a surplus of power from the electricity. The hydrogen is stored to be used in a fuel cell, which uses oxygen from the air and hydrogen from the gaseous state for the generation of electricity. Long-term energy storage is possible when using hydrogen [7-8]. The efficiency models of HESS are given as (3) and (4).

$$P_{EL}=\eta_{EL}\times P_{wpp}, \tag{3}$$

$$P_{FC}=\eta_{FC}\times P_{EL}. \tag{4}$$

Fuel cells and the electrolyzer's efficiency are provided by [4]. HESS charging and discharging are carried out by the matrix, demonstrated in (5) and (6).

$$\mathbf{ch}=\left[P_{EL,1},\ldots,P_{EL,h},\ldots,P_{EL,24}\right], \quad \text{for } h=1,2,3,\ldots,24, \tag{5}$$

$$\mathbf{dch}=\left[P_{FC,1},\ldots,P_{FC,h},\ldots,P_{FC,24}\right], \quad \text{for } h=1,2,3,\ldots,24. \tag{6}$$

III. PSO-Based ODS Algorithm

PSO is a swarm intelligence technique for nonlinear function optimization. The idea is to simulate the actions associated with a swarm of particles, each of which could provide a potential solution for the optimization problem. The particles traverse a search space, repositioning themselves in both the swarms and their own best-known placements. The objective is to iteratively update the particle locations to find the best solution [9].

A. Objective Function

Our suggested approach in this work is to minimize *DL* considering the penalty function for constraints violation, which can be represented as (7),

$$\text{minimize} \quad DL=\sum_{h=1}^{24}P_{loss,h}+PN. \tag{7}$$

When calculating $P_{loss,h}$, the process involves determining the value through power flow calculations represented as (8),

$$P_{loss,h}=\sum_{i=1}^{NB}\sum_{\substack{j=1\\ j\neq i}}^{NB}G_{ij}\left[(V_{i,h})^2+(V_{j,h})^2-2V_{i,h}V_{j,h}\cos(\delta_{i,h}-\delta_{j,h})\right], \quad \text{for } i,j=1,2,3,\ldots,\text{NB}, h=1,2,3,\ldots,24. \tag{8}$$

The constraints for HESS limitations are,

$$P_{FC,\min} < P_{FC} < P_{FC,rated}, \quad (9)$$

$$P_{EL,\min} < P_{EL} < P_{EL,rated}, \text{ and} \quad (10)$$

$$E_{tank,\min} < E_{tank} < E_{tank,rated}. \quad (11)$$

In the first step, the storage level is determined by a value that relies on the lowest and highest storage capacity. Mathematically, the associated storage levels for the following time intervals have been defined as follows:

$$E_{tank,h} = E_{tank,h-1} + \mathbf{ch}(h) - \mathbf{dch}(h). \quad (12)$$

The scheduling of **ch** and **dch** in (5) and (6) is obtained by PSO. The matrix **ch** and **dch** are used for acquiring *DL* in (7); the scheduling was updated by the PSO. The objective function is to minimize *DL*, which is obtained by load flow analysis. The term "gbest" refers to the minimum value of *DL* among all particles, whereas "pbest" denotes the minimum *DL* of an individual particle [10]. The PSO-based ODS algorithms are illustrated in Figure 2.

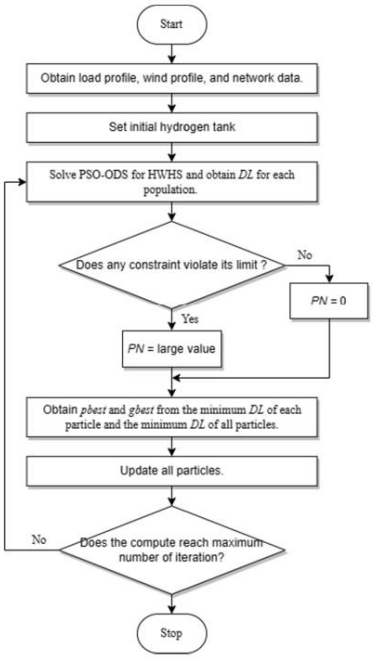

Fig. 2. The flow chart of the PSO-ODS for HWHS.

IV. Result And Disscusion

In this paper, two system case studies are investigated, including:

Case I: IEEE 33-bus system with WPP integrated.

Case II: IEEE 33-bus system with PSO-based ODS for HWHS.

The load profile of the northeastern region of Thailand and the wind speed profile from the Thai Meteorological Department are used, as observed in Figs.3 and 4. The reduction in *DL* between Case I and Case II is observed for comparison.

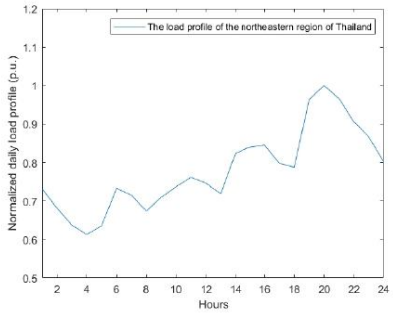

Fig. 3. The load profile of the northeastern region of Thailand

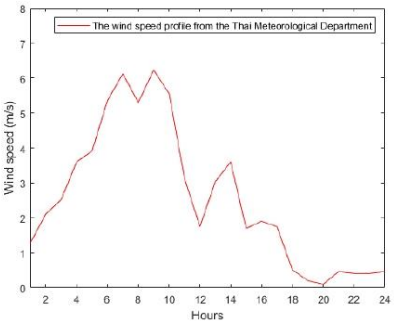

Fig. 4. The wind speed profile from the Thai Meteorological Department

A. IEEE 33-bus with WPP integrated

In this case, WPP connects to bus no. 26 [6] of the IEEE 33-bus radial distribution test system [11]. The number of wind turbines is 25. The system is modified as shown in Fig. 5.

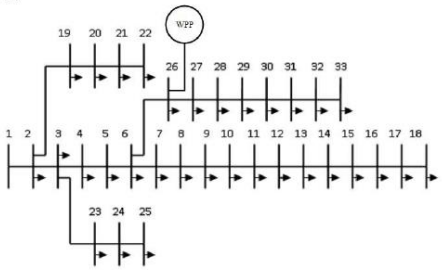

Fig. 5. The modified IEEE 33-bus radial distribution test system with WPP.

TABLE I. SPECIFICATION OF EWT DW 52-500 KW [12]

Parameters	Values
$P_{w,rated}$	500 kW
$v_{cut\text{-}in}$	3 m/s
$v_{w,rated}$	10 m/s
$v_{cut\text{-}off}$	25 m/s

The practical specifications of the EWT DW 52–500 kW wind turbine are used to simulate fluctuations in output power with wind speed [11–13]. The WPP is located at bus number 26 [6]. The specification of each wind turbine is given in Table I [12].

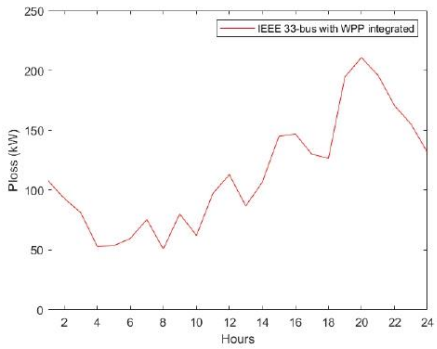

Fig. 6. The hourly power loss of IEEE 33-bus with WPP integrated.

Figure 6 displays the power loss for each hour of the modified IEEE 33-bus system with WPP integrated. WPP has an abundance of wind power during off-peak load times. Nevertheless, there is a shortage of wind during peak demand periods, which indicates that no real power from WPP can be injected into the system, leading to high power loss during peak hours. The result shows that *DL* in Case I is 2,727 kWh.

B. IEEE 33-bus system with PSO base ODS for HWHS.

In this case, HWHS connects to bus no. 26 of the IEEE 33-bus radial distribution test system [11]. Incorporating HESS into the structure provides a solution to wind fluctuation and uncertainty. Using HESS to minimize *DL* is the primary goal of this effort. In the simulation, the initial quantity of hydrogen is 20% of the tank's capacity. The system is modified as shown in Fig. 7. In each trial, the particle size is set at 100 particles, and the running iteration is 100 iterations. The convergence curve for *DL* solution is displayed in Fig 8.

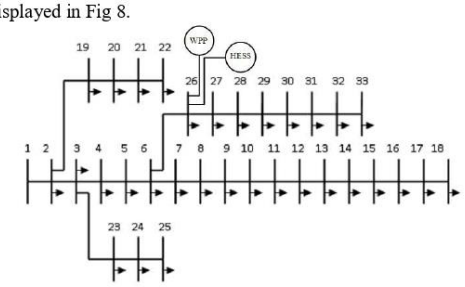

Fig. 7. The modified IEEE 33-bus radial distribution test system with HWHS.

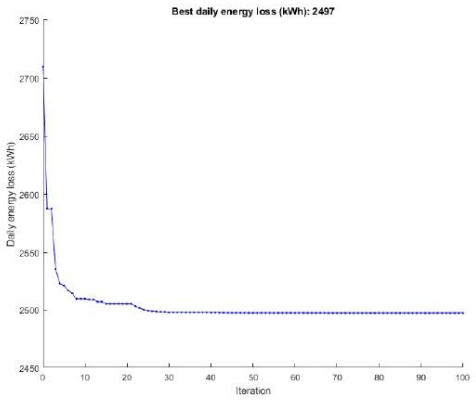

Fig. 8. The convergence of *DL* solution.

Figure 9. and Table II illustrate the outputs from 30 trials of Case II. The best and worst solutions are 2497.0002 kWh and 2497.0333 kWh, respectively. The average from 30 trials from Case II is 2497.0049 kWh. The solutions with 30 trials showed that the *DL* solutions are clustered. Therefore, the proposed tecnique is shown to be dependable and potentially find the optimal solution.

TABLE II. THE LOWEST, AVERAGE, AND HIGHEST *DL* FROM 30 TRIAL SOLUTIONS OF PSO-ODS FOR HWHS

	PSO-ODS FOR HWHS		
The daily energy loss (kWh)	***Lowest***	***Avg.***	***Highest***
	2497.0002	2497.0049	2497.0333

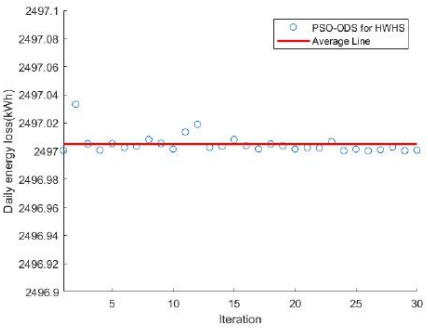

Fig. 9. The solution with 30 trials of PSO-ODS for HWHS.

The optimal scheduling of HESS is shown in Fig. 10. The scheduling is managed by the PSO algorithm to minimize energy losses. The HESS charges when $P_{wpp,h}$ is high, and in this interval is off-peak load time and discharging when peak

load time. The comparison results between Case I and Case II are shown in Fig. 11. As illustrated in Figs. 10 and 11, by using the proposed method, the HESS discharges between 3:00 p.m. and 12:00 a.m., which is the peak period. The HESS charges between 4:00 a.m. and 11:00 a.m. and between 1:00 p.m. and 2:00 p.m., which is the light load period. At 1:00 a.m. and 12:00 p.m., the HESS discharges power due to a shortage of wind power generation. This results in a significant decrease in real power loss.

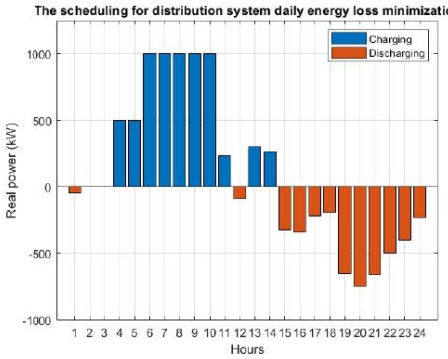

Fig. 10. The scheduling for distribution system *DL* minimization.

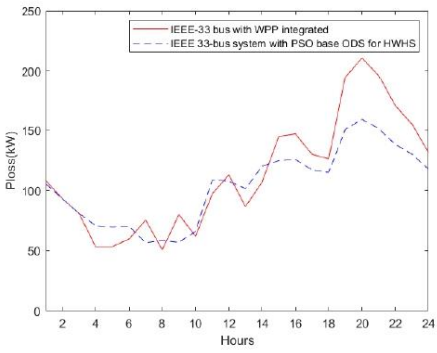

Fig. 11. The comparison of power loss between IEEE 33-bus with WPP integrated and IEEE 33-bus with PSO-ODS for HWHS.

The HESS parameters used in the simulations in Case II are shown in Table III.

TABLE III. THE PARAMETERS OF HESS ARE USED IN CASE II

Parameters	Values
$P_{FC,rated}$	1000 kW
$P_{EL,rated}$	1000 kW
$E_{tank,rated}$	10000 kWh

V. CONCLUSION

In this paper, the ODS using PSO for HWHS to minimize *DL* is proposed. The proposed approach was assessed using an IEEE 33-bus radial distribution test system utilizing the load profile of the northeastern region of Thailand and the wind speed profile of the Thai Meteorological Department. The system case studies are separated into two cases. The case where HWHS is integrated into the system illustrates that there is energy arbitrage using HESS to discharge the real power into the system when the system has peak load time and charging during times of light load, and wind power is plentiful. The result showed that the proposed method can effectively minimize *DL* and efficiently utilize the HWHS.

ACKNOWLEDGMENT

We extend our sincere appreciation to Suranaree University of Technology, Thailand, for their scholarship and facilities provided throughout this research endeavor. Their invaluable support greatly influenced the successful culmination of this study.

REFERENCES

[1] M. Shatnawi, N. A. Qaydi, N. Aljaberi and M. Aljaberi, "Hydrogen-Based Energy Storage Systems: A Review," 2018 7th International Conference on Renewable Energy Research and Applications (ICRERA), Paris, France, 2018, pp. 697-700, doi: 10.1109/ICRERA.2018.8566903.

[2] Z. Hong, Z. Wei, and X. Han, "Optimization scheduling control strategy of wind-hydrogen system considering hydrogen production efficiency," *Journal of Energy Storage*, vol. 47, p. 103609, Mar. 2022, doi: 10.1016/j.est.2021.103609.

[3] L. Valverde, F. J. P. Lucena, J. Guerra, and F. Rosa, "Definition, analysis and experimental investigation of operation modes in hydrogen-renewable-based power plants incorporating hybrid energy storage," *Energy Conversion and Management*, vol. 113, pp. 290–311, Apr. 2016, doi: 10.1016/j.enconman.2016.01.036.

[4] O. Utomo, M. Abeysekera, and C. E. Ugalde-Loo, "Optimal operation of a hydrogen storage and fuel cell coupled integrated energy system," *Sustainability*, vol. 13, no. 6, p. 3525, Mar. 2021, doi: 10.3390/su13063525.

[5] G. He, Z. Wang, H. Ma, and X. Zhou, "Optimal capacity configuration of Wind–Solar hydrogen storage microgrid based on IDW-PSO," Batteries, vol. 9, no. 8, p. 410, Aug. 2023, doi: 10.3390/batteries9080410.

[6] S. Paul, H. Karbouj and Z. H. Rather, "Optimal Placement of Wind Power Plant in a Radial Distribution Network Considering Plant Reliability," 2018 International Conference on Power System Technology (POWERCON), Guangzhou, China, 2018, pp. 2021-2026, doi: 10.1109/POWERCON.2018.8601946.

[7] H. Eskandari, M. Kiani, M. Zadehbagheri, and T. Niknam, "Optimal scheduling of storage device, renewable resources and hydrogen storage in combined heat and power microgrids in the presence plug-in hybrid electric vehicles and their charging demand," Journal of Energy Storage, vol. 50, p. 104558, Jun. 2022, doi: 10.1016/j.est.2022.104558.

[8] S. O. Amrouche, D. Rekioua and T. Rekioua, "Overview of energy storage in renewable energy systems," 2015 3rd International Renewable and Sustainable Energy Conference (IRSEC), Marrakech, Morocco, 2015, pp. 1-6, doi: 10.1109/IRSEC.2015.7454988.

[9] J. Kennedy and R. Eberhart, "Particle swarm optimization," Proceedings of ICNN'95 - International Conference on Neural Networks, Perth, WA, Australia, 1995, pp. 1942-1948 vol.4, doi: 10.1109/ICNN.1995.488968.

[10] K.Kaiyawong and K.Chayakulkheeree, "Coordinated optimal placement of energy storage system and capacitor bank considering optimal energy storage scheduling for distribution system using Mixed-Integer Particle swarm optimization," International Journal of Intelligent Engineering and Systems, vol. 15, no. 2, pp. 329–337, Apr. 2022, doi: 10.22266/ijies2022.0430.30.

[11] P. S. Meera and S. Hemamalini, "Optimal Siting of Distributed Generators in a Distribution Network using Artificial Immune System," International Journal of Electrical and Computer Engineering, vol. 7, no. 2, p. 641, Apr. 2017, doi: 10.11591/ijece.v7i2.pp641-649.

[12] EWT, "Wind turbines," *EWT*, Dec. 18, 2018. https://ewtdirectwind.com/turbines/

[13] E. Beshr, H. A. Abdelghany, and M. Eteiba, "Novel optimization technique of isolated microgrid with hydrogen energy storage," *PLOS ONE*, vol. 13, no. 2, p. e0193224, Feb. 2018, doi: 10.1371/journal.pone.0193224.

Optimal scheduling of multi-energy systems with wind-solar power and hydrogen storage integration

Suttipong Dechjinda[1], Keerati Chayakulkheeree [1,*]

ARTICLE INFO

Article history:
Received:
Revised:
Accepted:

Keywords:
Optimal scheduling
Multi-energy systems
Hydrogen storage
Energy hubs
Wind-solar power

ABSTRACT

This paper presents an optimization framework for scheduling a grid-connected multi-energy system that converts electricity from the power grid and natural gas to electricity and heat consumption, integrating wind-solar power and hydrogen storage. The study aims to develop a model that efficiently schedules energy usage while accounting for excess wind-solar power utilization, storage capabilities, and hydrogen scheduling. By incorporating dynamic pricing mechanisms, such as real-time pricing, and a stochastic model to address load fluctuations during peak periods, the proposed method provides a more realistic and adaptive approach to energy management. A combination of linear programming (LP) and particle swarm optimization (PSO) is employed to balance supply demand and minimize total operating costs. The results demonstrate significant improvements in coordinated operation efficiency and cost savings under various scenarios. Additionally, although the proposed technique demonstrates faster convergence, it requires longer runtime computation while delivering a more near-optimal global solution compared to conventional PSO. This framework offers a solution for enhancing efficiency, cost reduction, and operational flexibility of multi-energy systems, paving the way for a more sustainable and economically viable energy future.

1. INTRODUCTION

In the modern era, the incorporation of several different energy systems that are composed of many energy carriers is paving the way for a more sustainable future [1]. One of the most significant characteristics of this system is that it has multiple energy carriers, not only electricity. Synergies among different types of energy are seen to provide a substantial capability for system development [2, 3]. In addition to the possibilities of modern technology, state-of-the-art, emerging, and upcoming energy technologies, such as fuel cell (FC), are considered [4]. The multi-energy system (MES) is the solution to decrease the operating cost and promote carbon neutrality. The energy hub (EH) concept is used to consider efficiently supplying energy in each section using many kinds of energy. The EH infrastructure was first discovered in [2], and the basic concept of an EH is shown in Fig. 1. However, this concept will achieve the main goal of industrial, commercial, and residential consumers emphasizing how to minimize total operating costs (TOC) [5].

The trending technology in the MES with the EH model is combined heat and power (CHP) such as micro-turbine (MT) can dispatch two energies consisting of heat and electricity energy, power-to-gas (PtG) such as electricity energy to hydrogen gas, and gas-to-power (GtP) such as hydrogen gas to electricity energy [6, 7]. In this framework, PtG technology converts renewable energy (RE) to hydrogen gas by electrolyzer (EL). When RE generates excess energy, it can be utilized, stored, or distributed when it is synergized with a system called "Hydrogen Storage (HS)". GtP technology converts hydrogen gas to electricity energy via FC in HS. CHP technology dispatches electricity and heat demand by fueling natural gas (NG) [8, 9].

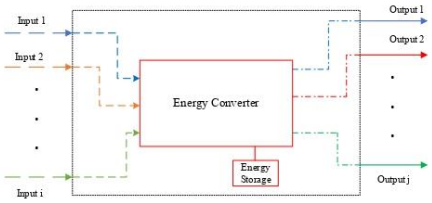

Fig. 1. The basic concept of an EH

Hydrogen production is defined in various color codes depending on the manufacturing process and cleanliness. It can be categorized into five colors: grey, brown, blue, turquoise, and green hydrogen [10]. Grey hydrogen is

[1]*School of Electrical Engineering, Suranaree University of Technology, Nakhonratchasima, 30000, Thailand.*
**Corresponding author:* Keerati Chayakulkheeree; Email: keerati.ch@sut.ac.th

produced from fossil fuels such as NG through steam reforming, emitting around 10 tons of CO_2 during the process [10, 11]. It's commonly used in petroleum-based chemicals and ammonia production. Brown hydrogen, derived from coal gasification, also releases significant CO_2. Blue hydrogen mitigates these emissions by employing carbon capture and storage. Turquoise hydrogen, generated via methane pyrolysis, produces solid carbon soot instead of CO_2. Green hydrogen, the cleanest, is produced using RE sources, such as wind or solar but faces challenges related to system efficiency and energy intermittent. Integrating HS can address these challenges [10]–[13].

Consequently, a significant amount of research has been proposed on MES with the EH model. Thanh-tung et al. [9] proposed a model of residential area load including electricity and heat from dispatching a multi-energy source (electricity and NG). Using mixed integer programming (MIP) based-general algebraic modeling system (GAMS) software to minimize the energy usage cost. The optimal results show that off-peak energy demand is primarily supplied by the grid, while normal and peak-hour demand is partially met by converting energy from NG to electricity, reducing system peaks, and lowering customer costs. The integration of multiple energy types improves electricity supply reliability. Then, Ha et al. [14] presented an integrating battery energy storage systems (BESS), photovoltaic panels (PVP), and solar energy model for residential areas. The case study is divided into four scenarios, each comprising variations such as with or without BESS and PV systems. The energy usage cost minimization using MIP-GAMS illustrates that the result in each case is decreasing. When PVP and BESS are integrated, the TOC is lowest. Moreover, Liu et al. [15] studied an EH model in different energy integrated. The study separated three kinds of EH cases to assess how different combinations of energy equipment. The components of EH include a boiler, cogeneration unit, chiller boiler, electric heat pump, and energy storage to dispatch electricity, heat, and cooling demand from electricity and NG as a source. The optimization process aims to minimize the TOC of the energy system, ensuring efficient energy utilization and balancing between different energy sources. The result shows that the optimal EH configuration is the most collaborative of energy. It can significantly reduce energy costs by coupling electricity, gas, and heat networks while optimizing the use of equipment like CHP and heat pumps. Additionally, Javadi et al. [16] focused on BESS integration to enhance the operational efficiency of a multi-carrier EH through optimal scheduling. The EH consists of various components, including micro-combined heat, electric heat pumps, boilers, absorption chillers, and battery storage with the energy management problem modeled using mixed-integer nonlinear programming (MINLP). The optimization aims to reduce costs and improve battery life by considering energy prices and battery state of charge. Simulation results highlight the importance of optimizing energy storage, leading to lower operational costs, better load management, and improved system reliability. Also, Geng and Jia [17] proposed a hybrid genetic algorithm and particle swarm optimization (GA-PSO) strategy, which combines PSO with GA to solve the optimal operation of EH. The EH model is comprised of electricity storage and heat storage coordinated with a gas turbine, gas boiler, electric chiller, and absorption chiller to dispatch electricity, heat, and cooling demand. When comparing a proposed algorithm GA-PSO with the conventional PSO, the results emphasize that GA-PSO significantly enhances convergence capability while also demonstrating a better economy in optimizing EH operations. In addition, Wang [18] proposed the strategy of optimal scheduling for multi-energy microgrids that integrates electricity and thermal energy sources, considering demand response and BESS integration. Using MILP solved by CPLEX, the study simulates the operation of a grid-connected microgrid consisting of FC, wind turbines (WTs), PVP, and thermal storage. Three different energy dispatch schemes are tested, with the third scheme incorporating demand responses showing the best results. This scheme not only reduces operational costs but also turns grid interactions into profit opportunities by smoothing energy demand and optimizing the use of RE and storage. The research demonstrates how integrating demand responses can enhance system flexibility, lower costs, and promote sustainable energy use. Furthermore, Timothée et al. [19] investigated the optimal dispatch of a multi-storage and multi-energy hub, integrating PVP, WTs, boilers, internal combustion generators, and cogeneration plants, alongside both heat and electricity storage systems. The study employed an evolutionary algorithm (EA) for optimization and compared the results with PSO. Results highlighted the volatility in dispatch strategies, which could be mitigated by increasing battery storage capacity. The results indicate that both the battery and internal combustion generators are utilized to meet peak power demand and export electricity to the grid when prices are elevated. In terms of heat demand, the boiler operates at full capacity, with the cogeneration plants unit contributing a smaller portion of the heat supply compared to the boiler. The research emphasizes the importance of optimizing EH to manage demand, renewable variability, and grid interactions, ensuring cost-effective and efficient energy distribution.

As a result, infrastructure MES with EH necessitates a significant amount of research and development [20]–[24]. This paper proposes a multi-energy system with wind-solar power and hydrogen storage (MES-WSPHS), incorporating energy management strategies for dispatching electricity and heat demands. The framework accounts for electricity tariffs based on time-of-use (TOU) and a constant NG

price, while also evaluating the impact of dynamic pricing models, such as real-time pricing (RTP). In the proposed method, a hybrid particle swarm optimization and linear programming (PSO-LP) approach. The MES includes electricity from the power grid and NG is optimally scheduled by LP, on an hourly basis. Meanwhile, the integrated wind-solar power and HS system are optimally scheduled by PSO daily. At peak load times, Monte Carlo simulation (MCS) is used to assess the fluctuations in demand, providing a more practical analysis. Additionally, this framework addresses a research gap by proposing an EH model that fully integrates green hydrogen production from HS and utilizes PSO-LP which is a combination of metaheuristic algorithm and deterministic optimization techniques for finding the best solution.

Table 1. Research gap analysis

Works	Interconnect multi-energy				Algorithm					Type of H_2		Objective
	Electricity	NG	WTs- PVP	H_2	MIP		PSO	GA	EA	Grey	Green	
					MLP	MINLP						
[9]	✓	✓			✓							TOC
[14]	✓	✓			✓							
[15]	✓	✓			✓							
[16]	✓	✓				✓						
[17]	✓	✓					✓	✓				
[18]	✓	✓	✓		✓							
[19]	✓	✓	✓				✓		✓			
This work	✓	✓	✓	✓	✓ (LP)		✓				✓	

The rest of the paper is organized as follows: Section II delves into system modeling and its principal components, providing detailed mathematical modeling of MES-WSPHS, WTs, and PVP, which are a renewable resource, conversion technologies, and HS mechanisms. Section III details the PSO-LP techniques used to optimize scheduling with a focus on minimizing TOC and a load stochastic model at peak spot time is proposed. Section IV presents case-based scenario studies and simulations to evaluate the effectiveness of the proposed methods. Including simulation when using RTP to reflect practical market conditions. The stochastic model with MCS is utilized to demonstrate when the demands have a fluctuation condition [25]. Finally, Section V provides a comprehensive summary of the key findings, highlighting the most significant insights drawn from the analysis.

2. SYSTEM MODELLING

2.1. MES-WSPHS

For system modeling, the components of MES-WSPHS are shown in Fig. 2. The input part consists of an electricity grid and NG to dispatch energy to the output which is electricity and heat demands. The conversion technology, which is the center of EH includes a transformer (TR), gas boiler (GB), MT, WTs, and PVP. With HS, the excessive RE can be converted to hydrogen and stored for utilization at the proper period. As a result, the resources can be coordinately utilized, leading to higher overall efficiency. In Fig. 2, electricity (P_E) and NG (P_{NG}) serve as the primary input power for the system and must supply the required electricity demand (L_E) and heat demand (L_H), respectively [5]. Conversion efficiency is considered and can be mathematically expressed as shown in (1).

$$\begin{bmatrix} L_E \\ L_H \end{bmatrix} = \begin{bmatrix} \eta_{TR} & \eta_{MT}^{E} & 0 \\ 0 & \eta_{MT}^{H} & \eta_{GB} \end{bmatrix} \begin{bmatrix} P_E \\ P_{NG}^{1} \\ P_{NG}^{2} \end{bmatrix} + \begin{bmatrix} P_{WPS} + P_{FC} \\ 0 \end{bmatrix}. \quad (1)$$

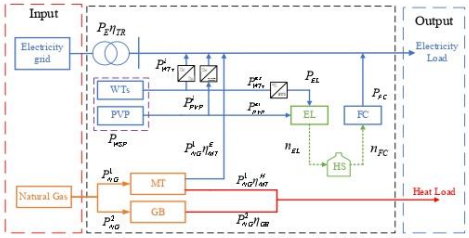

Fig. 2. The components of MES with EH model

2.2. WTs and PVP modeling

In a wind speed profile, the wind speed must be evaluated at a height corresponding to the turbine's cross-sectional area. Therefore, equation (2) illustrates a calculation for estimating wind speed at this altitude based on the power law theory [26].

$$\frac{v_{WT}(h)}{v_{WT,r}(h)} = \left(\frac{z}{z_r}\right)^{\alpha}. \quad (2)$$

A wind turbine generates electricity when the wind speed is above the cut-in speed or below the cut-off speed, otherwise the turbine produces no power. The power output increases with the cube of the wind speed divided by the rated wind speed when the wind speed is between the cut-in speed and the rated wind speed. Once the wind speed reaches the rated level, the turbine generates a constant rated power until the cut-off speed is reached. Above the cut-off speed condition, it is shut down to prevent damage. A wind turbine power output can be expressed (3) [27]:

$$P_{WT}(h)=\begin{cases}0 \quad \text{for} \quad 0<v_{WT}(h)<v_{cut-in},\\ P_{WT,rated}\times\left(\dfrac{v_{WT}(h)}{v_{WT,rated}}\right) \quad \text{for} \quad v_{cut-in}<v_{WT}(h)<v_{WT,rated},\\ P_{WT,rated} \quad \text{for} \quad v_{WT,rated}<v_{WT}(h)<v_{cut-off},\\ 0 \quad \text{for} \quad v_{WT}(h)<v_{cut-off}.\end{cases} \tag{3}$$

The total wind power per hour from (3), can be determined as the sum of each wind turbine, which can be modeled in (4).

$$P_{WTs}(h)=\sum_{k=1}^{NT}P_{WT,k}(h). \tag{4}$$

The PVP can be modeled as (5) which considers solar energy convert into electrical energy. The output is DC power and needs to be converted into AC power through an inverter [28].

$$P_{PVP}(h)=A\times\beta\times SI(h). \tag{5}$$

When the wind and solar power are excessed, it can be stored in the form of hydrogen. Therefore, the grid-injected wind and solar power at time h can be shown in (6)-(11).

$$P_{WTs}(h)=P_{WTs}^{i}(h)+P_{WTs}^{ex}(h), \tag{6}$$

$$P_{PVP}(h)=(P_{PVP}^{i}(h)\times\eta_{DC/AC})+P_{PVP}^{ex}(h), \tag{7}$$

$$P_{WSP}(h)=P_{WTs}(h)+P_{PVP}(h), \tag{8}$$

$$P_{WSP}^{ex}(h)=\begin{cases}0 & \text{if } P_{WSP}(\mathrm{h})\le \mathrm{L}_{E}(\mathrm{h})\\ P_{WSP}(h)-L_{E}(h) & \text{if } P_{WSP}(h)>L_{E}(h)\end{cases}, \tag{9}$$

$$P_{WSP}^{i}(h)=\begin{cases}P_{WSP} & if\ P_{WSP}(h)\le L_{E}(h)\\ L_{E}(h) & if\ P_{WSP}(h)>L_{E}(h)\end{cases}, \tag{10}$$

$$P_{EL}(h)=(P_{WTs}^{ex}(h)\times\eta_{AC/DC})+P_{PVP}^{ex}(h). \tag{11}$$

2.3. Conversion technologies

The conversion devices are TR, GB, and MT. In the electrical energy sector, TR is used to convert the grid voltage to the load. The TR efficiency model can be expressed as (12) when electricity flows through the TR to supply loads.

$$P_{TR}=P_{E}\eta_{TR}. \tag{12}$$

In the NG energy sector, GB and MT are employed to convert NG to power [9, 14]. The efficiencies of the GB and MT are utilized to determine the load supply from NG formed as in (13) and (14). When considering NG cost, the power from NG can be defined as (15).

$$P_{GB}=P_{NG}^{2}\eta_{GB}, \tag{13}$$

$$P_{MT}^{E,H}=\begin{cases}P_{NG}^{1}\eta_{MT}^{E}; \text{ for electricity output}\\ P_{NG}^{1}\eta_{MT}^{H}; \text{ for heat output}\end{cases}, \tag{14}$$

$$P_{NG}=P_{NG}^{1}+P_{NG}^{2}. \tag{15}$$

2.4. HS mechanism

HS has gained considerable attention in recent studies and research efforts. In these systems, hydrogen is produced by EL when the power generated by WTs and PVP exceeds the power demand and is stored as a chemical substance. This stored hydrogen can later be used in the FC, where it reacts with oxygen from the air to generate electricity in its gaseous state. HS enables long-term energy retention, as highlighted in [29]. By applying Faraday's law, the molar flow rate of hydrogen is produced by the EL. The FC turns hydrogen into electricity, and hydrogen consumption is directly proportional to its power output [1, 30]. The molar flow of EL and FC can be described as a function in (16) and (17), respectively.

$$n_{H_2,EL}=\frac{\eta_{EL}P_{EL}}{LHV_{H2}}, \tag{16}$$

$$n_{H_2,FC}=\frac{P_{FC}}{\eta_{FC}LHV_{H2}}. \tag{17}$$

In the operation of HS, FC and EL cannot be operated simultaneously. Therefore, Y_{EL} and Y_{FC} representing binary numbers (0,1) are introduced for FC and EL operating conditions as shown in (18) [1, 30].

$$Y_{EL}=\begin{cases}1 & \text{when } Y_{FC}=0\\ 0 & \text{when } Y_{FC}=1\end{cases}. \tag{18}$$

A key control variable in the HS system is the hydrogen tank pressure at each hour. The tank pressure reflects the amount of hydrogen contained in the storage vessels and molar flow from (16) and (17) are used to calculate the pressure at each hour. The pressure calculation for the hour h is dependent on the previous time step, as shown in (19) [1, 30].

$$p_{\text{tank}}(h)=p_{\text{tank}}(h-1)+\left(\frac{\Re T_{H_2}}{V_{H_2}}n_{H_2,EL}(h)-n_{H_2,FC}(h)\right). \tag{19}$$

3. PROBLEM FORMULATION

3.1. Objective function

The proposed method uses the PSO-LP technique to find the optimal scheduling of MES-WSPHS. The multiple energy deliveries are formed as variables on an hourly basis, to find the optimal solution for the system that makes it the minimum operating cost. The analysis considers the TOU tariff and RTP as separate factors throughout the day. Therefore, the objective function is to minimize total operating costs while accounting for the TOU tariff and RTP independently, with a penalty function incorporated to address any constraints violations, as shown in (20).

$$\text{Minimize TOC}=\sum_{h=1}^{24}(C_{E}(h)P_{E}(h)+C_{NG}(h)P_{NG}(h))+PNF. \tag{20}$$

Subjected to the power balance constraints in (21)-(22),

$$L_E(h) - P_{FC}(h) - P^i_{WSP}(h) = P_{TR}(h), \quad (21)$$

$$L_H(h) = P_{GB}(h) + P^H_{MT}(h), \quad (22)$$

and the limit constraints of each conversion device as demonstrated by (23)-(28),

$$0 \le P_{TR}(h) \le P_{TR,rated}, \quad (23)$$

$$0 \le P^{E,H}_{MT}(h) \le P^{E,H}_{MT,rated}, \quad (24)$$

$$0 \le P_{GB}(h) \le P_{GB,rated}, \quad (25)$$

$$0 \le Y_{EL} P_{EL}(h) \le P_{EL,rated}, \quad (26)$$

$$0 \le Y_{FC} P_{FC}(h) \le P_{FC,rated}, \text{ and} \quad (27)$$

$$p_{\text{tank,min}} \le p_{\text{tank}}(h) \le p_{\text{tank,rated}}. \quad (28)$$

In this paper, the initial pressure which is indicated in the content of the HS tank is set to the final pressure when the day is over, as shown in (29),

$$p_{\text{tank}}(h = \text{initial}) = p_{\text{tank}}(h = 24). \quad (29)$$

In addition, penalty function terms can handle some constraints, which can't define a lower and upper boundary such as (25) and (26). The penalty function can be defined as a Karush–Kuhn–Tucker condition (KKT) in (30)

$$PNF = \lambda_1[(p_{\text{tank}}(h) - p_{\text{tank,min}})^2 + (p_{\text{tank}}(h) - p_{\text{tank,rated}})^2] + \lambda_2[(p_{\text{tank}}(h = 24) - p_{\text{tank}}(h = initial)]^2. \quad (30)$$

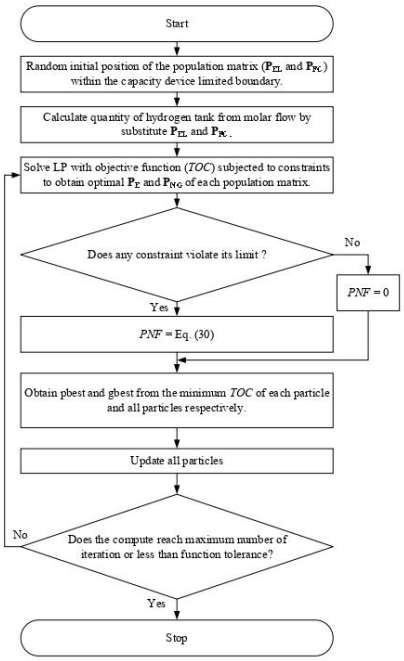

Fig. 3. The workflow of the PSO-LP technique under TOC

The operation of this work procedure, which involves calculating the objective function while handling constraints, follows the workflow depicted in Fig. 3

3.2. PSO-LP technique

The HS scheduling is a continuous variable (P_{EL} and P_{FC}), while the relation of power from the grid and NG (P_E and P_{NG}) can be formed as a linear problem. Therefore, we modify the mathematical formulation of the problem to account for utilizing a heuristic algorithm in the main loop and utilizing a deterministic algorithm in the subroutines. LP will optimize the problem in subroutines. Then, the main loop will be optimized by PSO. The overview concept of hybrid PSO-LP is shown in Fig. 4. The hybrid PSO-LP technique is an enhanced version of the traditional PSO algorithm, designed to be more efficient. The PSO is used for searching for optimal HS scheduling incorporating the optimal condition of electricity from the power grid and NG, under wind and solar power, electricity load, and heating load conditions.

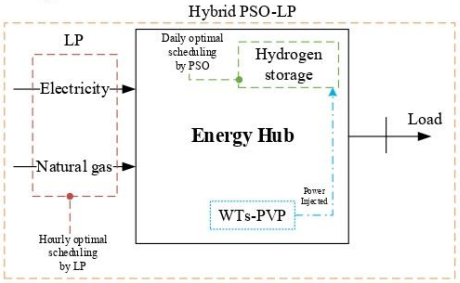

Fig. 4. The overview of hybrid PSO-LP

The PSO algorithm is a stochastic optimization technique inspired by the collective behavior of bird flocks and their emergent dynamics. In PSO, a population of potential solutions, referred to as particles, is used to search for the optimal result. This population is called a swarm, and each particle represents a possible solution. The algorithm begins by randomly assigning positions to the particles within the search space. These particles then update their positions in successive iterations, adjusting based on their velocities. Each particle keeps track of its best position, referred to as *pbest(i,h)*, and updates its velocity based on that. Particles also communicate with one another to adjust their movement. If a particle finds a solution better than its previous *pbest*, the value is replaced. Among the entire population, the best solution found is called the global best (*gbest*). In this paper, the population is formulated as follows (31) [31]:

$$\mathbf{P_{EL,FC}} = [P_{EL,FC}(1), P_{EL,FC}(2), ..., P_{EL,FC}(h), ..., P_{EL,FC}(24)]. \quad (31)$$

The matrix in (31) will solve the individual objective function simultaneously. Then this matrix is used to update

each particle's velocity as displayed in (32), and the next step of the matrix is updated by velocity as shown in (33) [31].

$$v(i,h+1) = wv(i,h) + c_1 rand_1(pbest(i,h) - \mathbf{P}_{EL,FC}(i,h)) + c_2 rand_2(gbest(i,h) - \mathbf{P}_{EL,FC}(i,h)), \quad (32)$$

$$\mathbf{P}_{EL,FC}(i,h+1) = \mathbf{P}_{EL,FC}(i,h) + v(i,h+1). \quad (33)$$

3.3. Stochastic load model

In practical terms, electricity and heat loads fluctuate based on user activity. Consequently, at the peak electricity and heat loads can be probabilistically modeled using a normal distribution. The normal distribution is a widely utilized probability density function (PDF) that represents continuous random variables with a characteristic bell-shaped curve. The PDF of the normal distribution is given by [32]:

$$f_{L_E}(L_E) = \frac{1}{\sqrt{(2\pi)\sigma_{L_E}}} \exp\left(-\frac{(L_E - \mu_{L_E})^2}{2\sigma_{L_E}}\right), \quad (34)$$

$$f_{L_H}(L_H) = \frac{1}{\sqrt{(2\pi)\sigma_{L_H}}} \exp\left(-\frac{(L_H - \mu_{L_H})^2}{2\sigma_{L_H}}\right). \quad (35)$$

4. RESULTS AND DISCUSSION

This section presents the data and simulation results for four case studies. MATLAB programming is used to develop an optimal daily scheduling algorithm for the proposed MES-WSPHS. Each case represents a distinct scenario, such as the inclusion of HS and coordination between electricity and NG systems. Different scheduling scenarios are analyzed.

4.1. Data acquired and assumptions

To evaluate the performance and feasibility of the MES-WSPHS configuration, it is essential to analyze the efficiency and capabilities of its individual components as shown in Table 2 [8, 20]. The electricity load profile utilized in this study was obtained from a typical summer day in the northeastern region of Thailand, with a peak load defined at 2 MW [27] as shown in Fig. 5(a). The heat load profile was acquired from [33] as illustrated in Fig. 5(b). The wind and solar profile were derived from data collected on a summer day in Pakchong, Thailand [27] .

This study examines a wind power system with four turbines rated at 500 kW each (NT = 4), as shown in Fig. 6. Subplots 1 and 2 in Fig. 6 illustrate wind speed conversion to power. Hourly solar irradiance and PVP output are shown in Fig. 7, subplots 1 and 2, respectively. Fig. 8 highlights excess wind and solar power over demand. Electricity costs follow TOU tariffs [34], while NG prices remain constant. Furthermore, RTP, which reflects dynamic price adjustments, both are described in Fig. 9

Table 2. The efficiency and rated device of each component

List	Component	Efficiency	Rated
No.1	Transformer	98%	2500 kVA
No.2	Electrolyzer	70%	500 kW
No.3	Fuel cell	60%	500 kW
No.4	Micro-turbine	40%, 50%	500 kW
No.5	Gas boiler	88%	1600 kW
No.6	Converter	95%	-
No.7	Pressure tank	-	100 bar

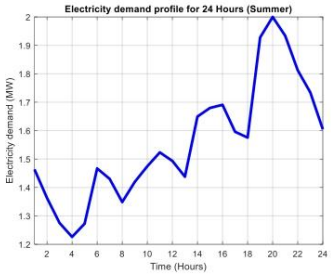

(a)

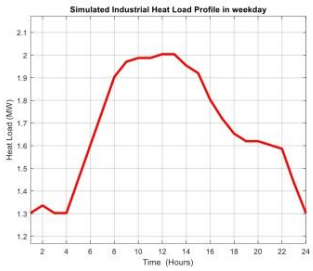

(b)

Fig. 5. The load profile (a) electricity (b) heat

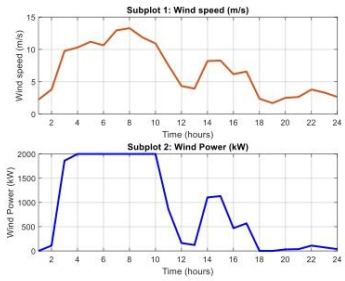

Fig. 6. The wind profile

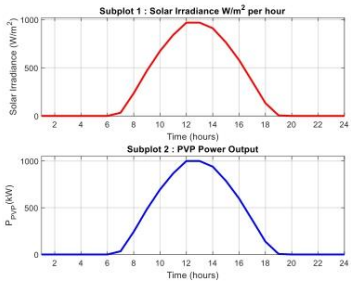

Fig. 7. The solar profile

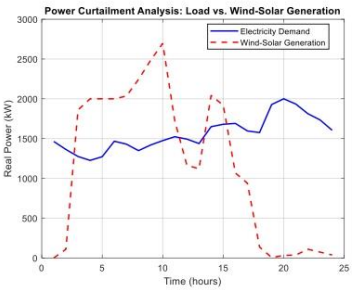

Fig. 8. The excess wind-solar generation

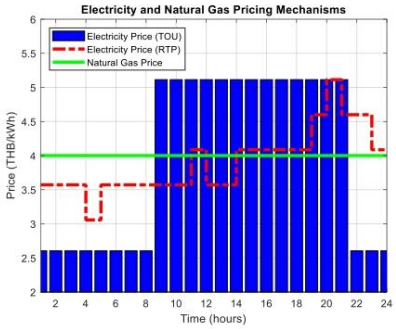

Fig. 9. The electricity and natural gas pricing mechanism

4.2. The simulation results

The case studies, illustrated in Fig. 10, are divided into four scenarios for analysis, as follows:

Case I: MES-WSP without HS, operating with uncoordinated electricity and NG under TOU tariffs.

Case II: MES-WSP with HS, but without coordinated operations between electricity and NG, under TOU tariffs.

Case III: MES-WSP with coordinated operations between electricity and NG, but without HS, under TOU tariffs.

Case IV: MES-WSP with HS and coordinated electricity and NG operations, under TOU tariffs.

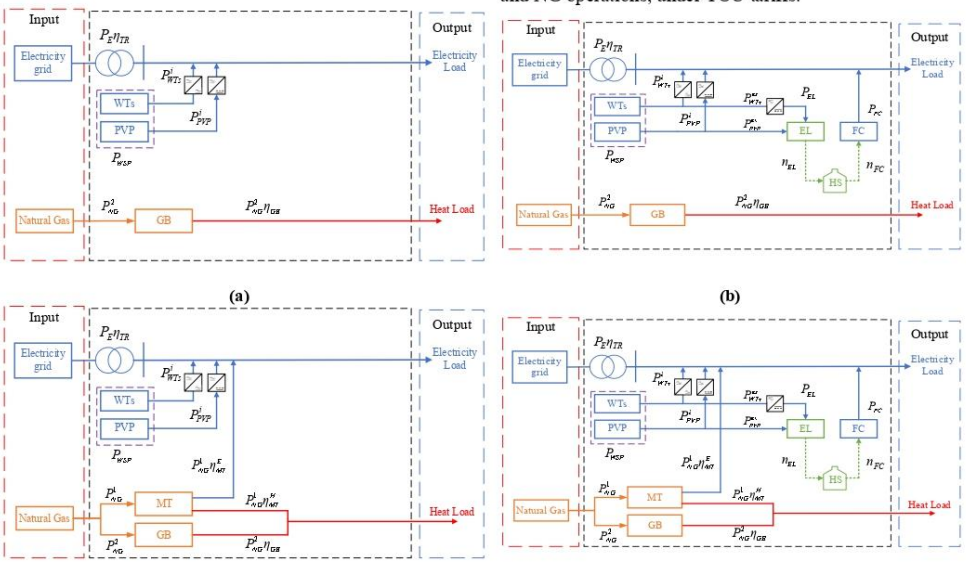

Fig. 10. Illustration of each case study (a) Case I, (b) Case II, (c) Case III, and (d) Case IV

In each case, the scheduling of energy proportions varies depending on the scenario. For cases without HS, only LP is employed to find the solution since there are no variables for the FC and EL. However, in scenarios incorporating HS, a hybrid PSO-LP method is utilized. This approach first optimizes the operation of the fuel cell and EL using PSO, and the results are subsequently processed using LP. The scheduled energy output for each component, as well as the costs associated with each energy sector, are summarized in Table 3. Furthermore, since HS is considered in Cases II and IV, with PSO-LP employed to derive the solutions, Figs. 11 to 16 provide detailed insights into the power balance, optimization algorithm, and the impact of HS on the proposed system. The figures are organized by case: (a) Case II and (b) Case IV, and they highlight the effectiveness of the proposed optimization in achieving optimal solutions. While demonstrating the role of HS integration with and without coordinated operation of NG-electricity to balance multiple types of energy with energy demand. However, in case of MT integration, more power loss occurs from operation efficiency than without MT integration but helps to significantly reduce TOC.

Table 3 Summary of power scheduling and energy costs for each sector

Case	Energy scheduling (kWh)									Operation costs (THB)		
	Energy through components					Demand-side				Electricity	NG	Total
	TR	MT	WSP	FC	GB	Gen	Used	Loss	Curtailed			
1	16,956	-	27,835	-	40,130	90,382	77,530	5,818	7,034	68,887	182,410	251,297
2	15,024	-		1,933		84,996		5,779	1,687	61,711	182,410	244,121
3	15,356	3,600		-	38,130	90,679		5,913	7,236	60,538	189,319	249,857
4	13,424	3,600		1,933		85,090		5,873	1,687	50,453	189,319	239,772

Various energy sources are utilized to meet output demands through multiple energy scheduling in the EH. In Table 3, Case I represents no cooperation between electricity and NG systems, where each sector operates independently, focusing solely on its efficiency. Conversely, Case III involves coordinated operation between electricity and NG, with NG being used to dispatch the electricity load via MT to reduce electricity consumption. Excess wind and solar power, as shown in Fig. 8, is not utilized, resulting in no additional energy savings.

Case II integrates HS without coordination with the electricity and NG systems, whereas Cases IV incorporates both HS and coordinated operation, referred to as MES-WSPHS. This significantly enhances energy management strategy since HS stores excess wind and solar energy, which is then discharged at other times. The power balance in each energy sector is depicted in Fig. 11(a) and 11(b) for electricity and in Figs. 12(a) and 12(b) for heat. Both Figs 11 and 12 focus exclusively on cases involving HS integration.

The energy flow through the MT, which operates in Cases III and IV produces both electricity and heat. In Case III and Case IV, the MT is scheduled to operate from 12 a.m. to 9 p.m. During these periods, NG costs are lower than the peak electricity costs in TOU tariffs. However, when energy generation is sufficient to meet demand, the MT does not operate in that hour. Figs 11(b) and 12(b) show the NG through MT do not operate at 2 p.m. and 3 p.m.

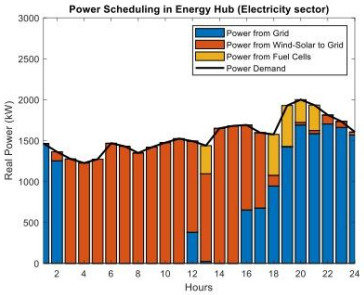

(a)

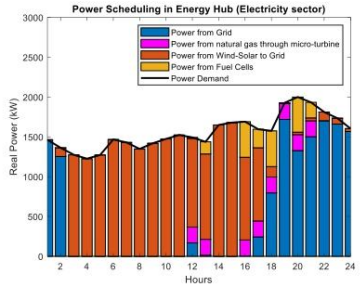

(b)

Fig. 11. Power scheduling in EH (electricity sector) (a) Case II and (b) Case IV

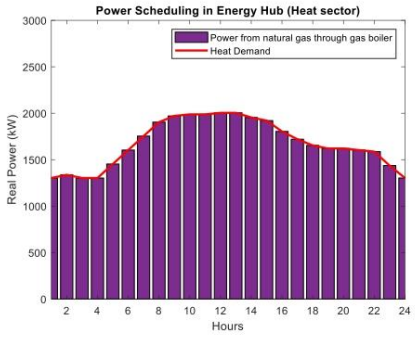

(a)

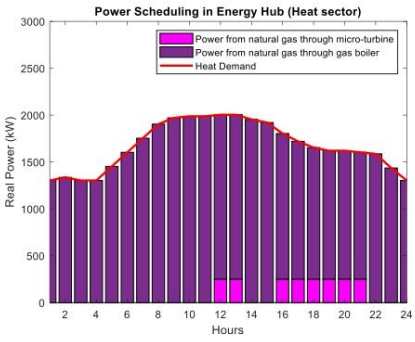

(b)

Fig. 12. Power scheduling in EH (heat sector) (a) Case II and (b) Case IV

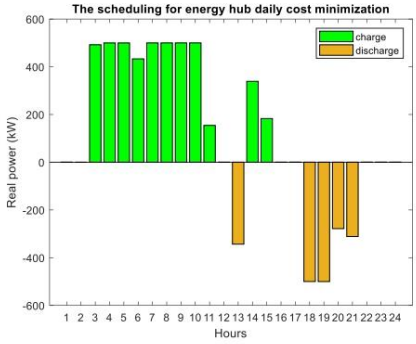

(a)

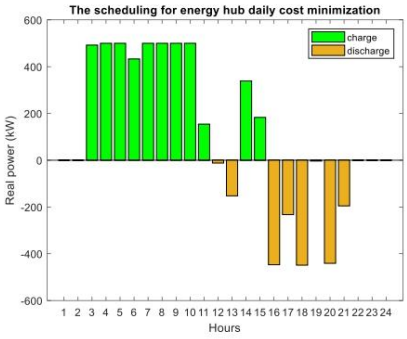

(b)

Fig. 13. HS scheduling for 24 hours ((a) Case II and (b) Case IV

Case II and Case IV with HS integration, EL turns an excess wind and solar power from 3 a.m. to 11 a.m. and 2 p.m. to 3 p.m. to HS. Then FC turns hydrogen into electricity to reduce electricity from the grid, the schedule of HS operation varies from case to case. Case II and Case IV have different patterns of FC scheduling. However, the power from FC operated is performing in the peak electricity costs period to reduce energy from the grid, resulting in a lower TOC and energy curtailment. The TOU tariff is utilized to define the objective, resulting in the FC operating as illustrated in Fig. 13 (a) Case II and (b) Case IV. In the study, the initial hydrogen tank pressure is set at 20 bar. During HS scheduling, the tank pressure is maintained within a range of no more than 100 bar and no less than 10 bar, which is defined in the state of the tank (SOT) is 100% and 0%, respectively. With the pressure at the final hour of the day equal to that of the initial hour. As shown in Fig. 14 (a) Case II and (b) Case IV, SOT is displayed as a percentage, representing the hydrogen energy storage model.

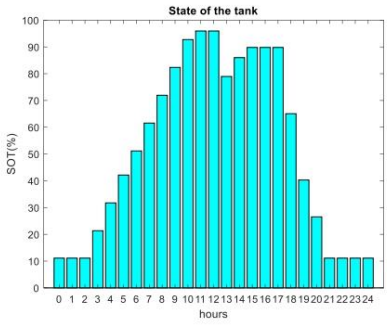

(a)

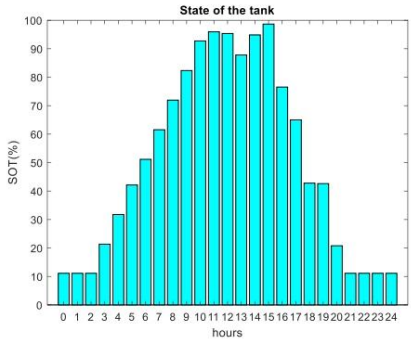

(b)

Fig. 14. State of the tank (%SOT) in HS
(a) Case II and (b) Case IV

Figure 15 (a), and (b) show the convergent PSO-LP solutions of Case II and Case IV, respectively. The best function value is TOC in both cases. Case II starts converging around 20 iterations and stops finding the optimal solution in 128 iterations. Case IV starts converging around 30 iterations and stops finding the optimal solution in 285 iterations. However, both cases can converge before the maximum iteration setting because the final solution is less than the function tolerance.

Figure 16 (a) and (b) demonstrate the results from 30 trials of Case II and Case IV which show the best, worst, and average lines of solutions, indicate that the fitness results of PSO-LP are clustered, with the standard derivations (SD) of 4.30 and 5.11, respectively. Therefore, the proposed method is demonstrated to be reliable and has the potential to find the optimal solutions.

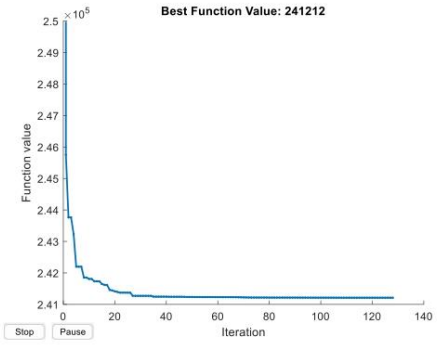

(a)

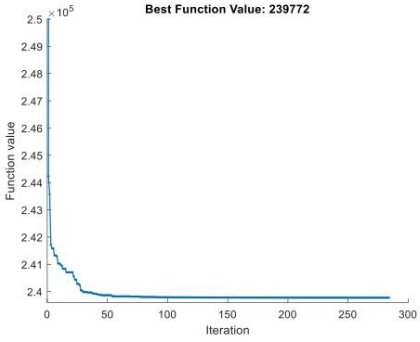

(b)

Fig. 15. The PSO-LP convergence plot
(a) Case II and (b) Case IV

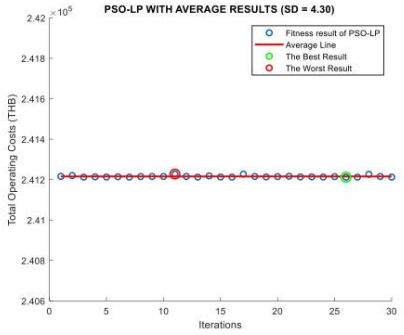

(a)

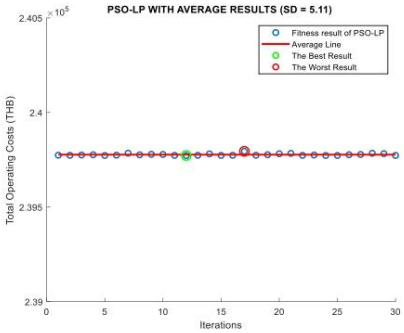

(b)

Fig. 16. The PSO-LP fitness results with 30 iterations
(a) Case II and (b) Case IV

4.3. MES-WSPHS with RTP mechanism

In this section, the impact of RTP on the operation of the MES-WSPHS is analyzed. The study investigates how dynamic electricity pricing influences the scheduling of various energy resources, ensuring cost-effective and efficient energy management. Fig. 17(a) and 17(b) illustrates the power scheduling for each energy sector. In the electricity sector, MT and HS are scheduled to operate between 7 p.m. and 10 p.m., that reflects the RTP mechanism indicates higher electricity prices during this period.

The integration of HS further enhances system flexibility, as depicted in Fig. 18(a), which illustrates the charge and discharge patterns of the HS system. It can be observed that hydrogen is primarily stored during low electricity price periods and discharged during peak price hours, aligning with the cost-minimization strategy. SOT is displayed in Fig. 18(b). The quantity of hydrogen in tank shows hydrogen reserves gradually increasing during the daytime and depleting as energy is discharged in the evening.

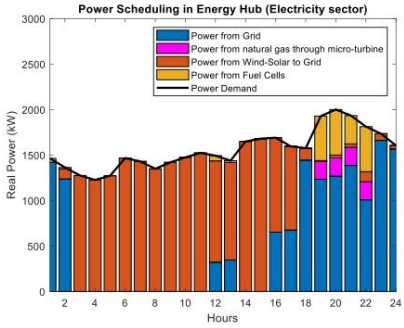

(a)

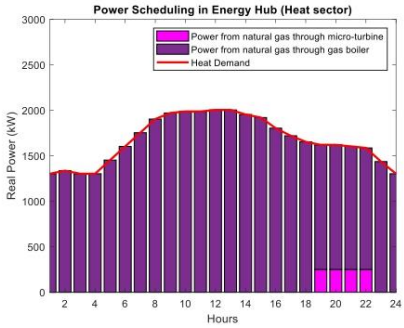

(b)

Fig. 17. Power scheduling in EH (a) electricity and (b) heat

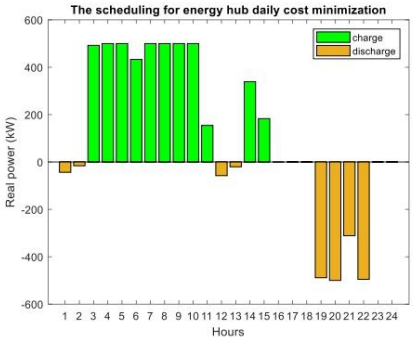

(a)

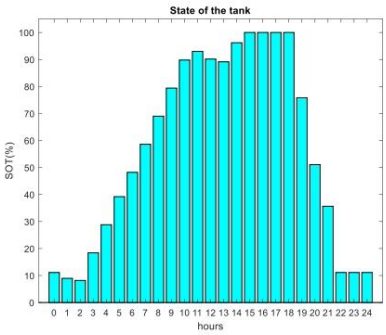

(b)

Fig. 18. (a) HS scheduling and (b) %SOT

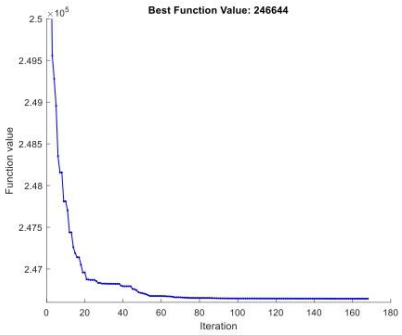

(a)

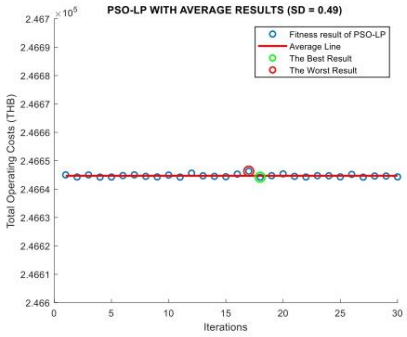

(b)

Fig.19. The PSO-LP (a) convergence plot and (b) fitness results with 30 iterations

Figure 19 (a) and (b) demonstrate the results from 30 trials of MES-WSPHS under RTP which show the best, worst, and average lines of solutions, indicate that the fitness results of PSO-LP are clustered, with the standard derivations (SD) of 0.49. This study is reliable and has the potential to find optimal solutions more than TOU tariff.

4.4. The comparison between PSO and PSO-LP

This section illustrates a different solution between the PSO and PSO-LP technique under the TOC as an objective function and demonstrated in Case IV. The aim is to highlight the performance of each approach that can minimize TOC effectively. To ensure a fair comparison between algorithms, the study established consistent parameters, as outlined in Table 4.

Table 4. The parameters of the PSO and PSO-LP settings

Variable	Settings
Swarm sizes	100
Iterations	500
Function Tolerance	$<10^{-6}$
w	[0.1,1.1]
c_1	1.49
c_2	1.49
$rand_1, rand_2$	[0,1]

Table 5. The runtime of the PSO and PSO-LP

Algorithm	Runtime (s)
PSO	611
PSO-LP	3,000

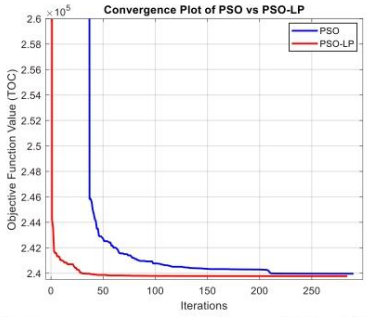

Fig. 20. Convergence comparison between PSO and PSO-LP

Figure 20 presents a comparison between PSO and PSO-LP, illustrating that both algorithms demonstrate similar convergence behavior. However, the proposed PSO-LP terminates the optimization process at 285 iterations, due to the predefined convergence criteria based on the tolerance between the current particle swarm and the previous swarm, with a function tolerance of less than 10^{-6}. This enables PSO-LP to achieve a near-optimal global solution. In contrast, PSO requires 291 iterations to terminate, taking slightly longer and failing to reach a near-optimal solution.

On the other hand, PSO-LP requires significant computational resources due to its two-step process: running PSO in the main loop and executing LP as a subroutine. This results in a longer runtime for PSO-LP compared to conventional PSO. Nevertheless, both algorithms are suitable for this problem, as the scheduling process must be completed within a day. The runtime details for this study are provided in Table 5.

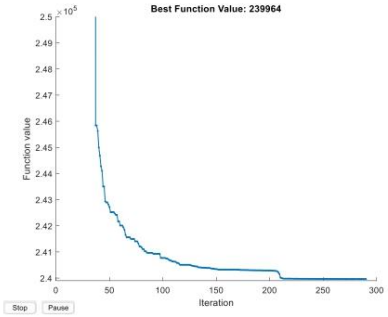

Fig. 21. The PSO convergence plot

The PSO convergence plot in Fig. 21 indicates a final TOC value of 239,964 THB, whereas the PSO-LP convergence plot in Fig. 15 (b) shows a final TOC value of 239,772 THB. This comparison highlights that PSO-LP achieves a more optimal solution than the conventional PSO algorithm.

4.5. MES-WSPHS with stochastic load model

The results of the Monte Carlo analysis demonstrate the effectiveness of the MES-WSPHS under varying stochastic load conditions at the peak time. Random load samples were generated until the tolerance criteria were satisfied, resulting in a probabilistic set of the load data. This dataset includes the mean value, standard deviation, and a fitting curve based on a normal distribution, allowing for an evaluation of the system's ability to adapt to uncertainty. Figure 22 shows the variability of the stochastic load at peak hour (one spotted), representing realistic fluctuations in demand. The peak electricity demand scenario represented by the stochastic load PDF for normal distribution is illustrated in Fig. 22. The parameter setting of MCS can be shown in Table 6.

Table 6. MCS parameters

Parameters	The mean value		The standard deviation	
	μ_E	μ_H	σ_E	σ_H
Values	$L_{E,\text{at E max}}$	$L_{H,\text{at E max}}$	$0.1\times\mu_E$	$0.1\times\mu_H$

When applying MCS to simulate the stochastic load model for determining the optimal scheduling of MES-WSPHS, the results, including TOC, electricity scheduling, and NG scheduling, are represented as PDF, as shown in Figs. 23 and 24. The convergence plot as shown in Fig 25 highlights the changes in the objective function with repeatability. The trend of the MCS procedure shows an increase as the number of iterations grows. Convergence analysis is essential for assessing the reliability of the proposed method and ensuring its ability to produce accuracy and uniform results.

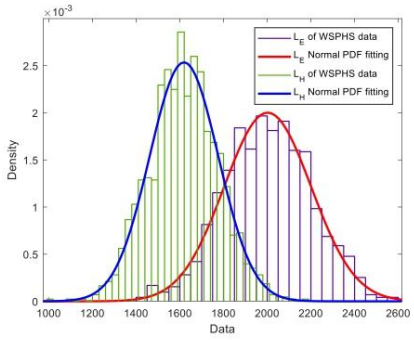

Fig. 22. Stochastic load PDF for MES-WSPHS at the peak electricity demand scenario

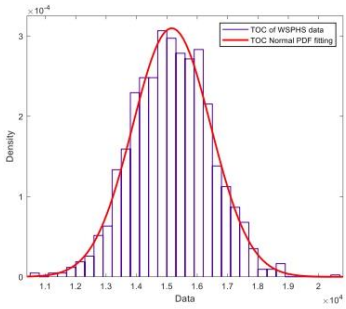

Fig. 23. Solution PDF for MES-WSPHS illustrates TOC at the peak electricity demand scenario

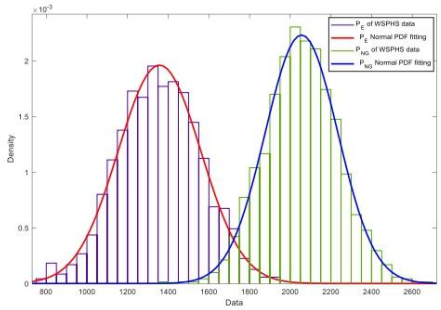

Fig. 24. Solution PDF for MES-WSPHS illustrates electricity and NG scheduling at the peak electricity demand scenario

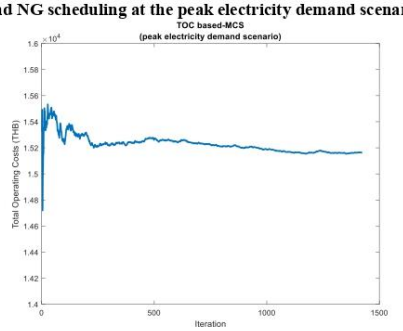

Fig. 25. The convergence plot TOC based-MCS at the peak electricity demand scenario

As a result, the proposed MES-WSPHS utilizes PSO-LP to determine the TOC minimization under TOU tariff and considers that, under probabilistic peak load conditions, the results can fit in a normal distribution perfectly. The mean value and the standard deviation of the normal distribution in each probabilistic variable follow in Table 7.

Table 7. The mean value and the standard deviation of the normal distribution

Parameters	The mean value (μ)	The standard deviation (σ)
L_E	2,001.95	199.356
L_H	1,619.01	157.347
P_E	1,357.02	203.425
P_{NG}	2,055.69	178.803
TOC	15,161.9	1,287.77

5. CONCLUSIONS

In this paper, the optimal scheduling of MES-WSPHS, using PSO-LP, to minimize TOC is proposed. The proposed approach was assessed using the MES with the EH model utilizing the electricity load profile of the northeastern region of Thailand, the wind speed and solar irradiance profile from one day in summer, and the heat load profile from the normalized profile of industry on weekdays. The study can be divided into four cases to thoroughly analyze the individual and combined impacts of HS and the coordination strategies between electricity and NG. The influence of RTP and the stochastic model is proposed to demonstrate a practical condition. Additionally, a comparison between conventional PSO and PSO-LP is discussed, highlighting that PSO-LP performs fast convergence and is more accurate than PSO under the same conditions. The results showed that the proposed method can effectively minimize TOC, enhance the economic operation of MES-WSPHS, and efficiently adapt to uncertainties and real-time price variations. The integration of RTP and stochastic modeling further emphasizes the robustness and practicality of the proposed approach in real-world scenarios.

ABBREVIATION

Variable

$\mathbf{P}$ = The matrix contains a scheduling variable.
η = Efficiency (%).
P = The power inputs or the power flow through the device (kW).
L = The power outputs or power demands (kW).
NT = The total number of wind turbines.
v = The velocity (m/s).
Y = The parameter indicates the operation state.
C = The cost of the energy input (THB/kWh).
PNF = The penalty functions.
λ = The Lagrange multiplier.
LHV = The low heat value (MJ/kmol).
$\Re$ = The gas constant (J/mol·K).
T = The mean temperature (K).
V = The volume (m^3).
p = The pressure (bar).
n = The molar flow (mol/s).
h = The times (hour).
z = The height (m).
α = The power law exponent.
A = Area of PVP installed (m^3).
β = PVP efficiency (%)
SI = Solar irradiance (W/m^2)
w = Inertia weight.
c = Learning factor.
$rand$ = A random number between 0 and 1.
$pbest$ = personal best.
$gbest$ = global best.
f = The probability density function.
σ = The standard deviation of the normal distribution.
μ = The mean value of the normal distribution.
SOT = The state of the tank (%).
TOC = The total operating costs (THB).

Subscript and Superscript

1 = The number which indicates the order.
2 = The number which indicates the order.
E = Electricity.
H = Heat.
NG = Natural gas.
H_2 = Hydrogen.
EL = Electrolyzer.
FC = Fuel cell.
MT = Micro-turbine.
TR = Transformer.
GB = Gas boiler.
WSP = Wind-solar power.
AC/DC = AC-to-DC converter.
DC/AC = DC-to-AC converter.
r = Reference.
WTs = Wind turbines.
i = Power injected into the grid.
ex = The excess power.
PVP = Photovoltaic panels.
tank = The storage of hydrogen.
$rated$ = The maximum limit.
min = The minimum limit.

ACKNOWLEDGEMENTS

We express our sincere gratitude to Suranaree University of Technology (SUT) for providing the essential resources and supportive environment that made this research possible.

REFERENCES

[1] M. L. Imeni; M. S. Ghazizadeh; M. A. Lasemi; and Z. Yang. 2023. Optimal Scheduling of a Hydrogen Based Energy Hub Considering a Stochastic Multi-Attribute Decision-Making Approach. Energies 16(2): 631.

[2] M. Geidl, G. Koeppel, P. Favre-Perrod, B. Klöckl, G. Andersson, and K. Fröhlich. 2007. The energy hub A powerful concept for future energy systems. Proceedings of the Third Annual Carnegie Mellon Conference on the Electricity Industry. Pittsburgh, PA, USA, 13–14 March. The Carnegie Mellon Electricity Industry Center.

[3] M. Geidl and G. Andersson. 2007. Optimal Power Flow of Multiple Energy Carriers. IEEE Transactions on Power Systems 22(1): 145-155.

[4] M. Lasemi and M. Ghazizadeh. 2023. Pave the Way for Hydrogen-Ready Smart Energy Hubs in Deep Renewable Energy System. Proceedings of the 2023 8th International Conference on Technology and Energy Management (ICTEM). Mazandaran, Babol, Iran, 8-9 February. IEEE Publisher.

[5] A. Zidan and H. A. Gabbar. 2016. Optimal scheduling of energy hubs in interconnected multi energy systems. Proceedings of the 2016 IEEE Smart Energy Grid Engineering (SEGE). Oshawa, ON, Canada, 21-24 August. IEEE Publisher.

[6] M. Qadrdan; M. Abeysekera; M. Chaudry; J. Wu; and N. Jenkins. 2015. Role of power-to-gas in an integrated gas and electricity system in Great Britain. International Journal of Hydrogen Energy 40(17): 5763-5775.

[7] N. C. Martin, F. V. Lith, and A. v. d. Molen. 2023. Remuneration and coordination aspects of flexibility by Power-to-Gas and Gas-to-Power technologies in distribution networks. Proceedings of the 27th International Conference on Electricity Distribution (CIRED 2023). Rome, Italy, 12-15 June. IET Publisher.

[8] T. Ha; Y. Xue; K. Lin; Y. Zhang; V. V. Thang; and T. Nguyen. 2022. Optimal Operation of Energy Hub Based Micro-energy Network with Integration of Renewables and Energy Storages. Journal of Modern Power Systems and Clean Energy 10(1): 100-108.

[9] H. Thanh-tung, Z. Yong-jun, H. Jian-ang, and V. V. Thang. 2016. Energy Hub modeling for minimal energy usage cost in residential areas. Proceedings of the 2016 IEEE International Conference on Power and Renewable Energy (ICPRE). Shanghai, China, 21-23 October. IEEE Publisher.

[10] A. I. Osman et al. 2022. Hydrogen production, storage, utilisation and environmental impacts: a review. Environmental Chemistry Letters 20(1): 153-188.

[11] M. Dvoynikov; G. Buslaev; A. Kunshin; D. Sidorov; A. Kraslawski; and M. Budovskaya. New Concepts of Hydrogen Production and Storage in Arctic Region. Resources 10(1): 3.

[12] A. b. Jumah. 2024. A comprehensive review of production, applications, and the path to a sustainable energy future with hydrogen. RSC Advances 14(36): 26400-26423.

[13] J. Zhang and J. Li. 2024. Revolution in Renewables: Integration of Green Hydrogen for a Sustainable Future. Energies 17(16): 4148.

[14] T. Ha; Y. Zhang; V. V. Thang; and J. Huang. 2017. Energy hub modeling to minimize residential energy costs considering solar energy and BESS. Journal of Modern Power Systems and Clean Energy 5(3): 389-399.

[15] J. Liu, P. Sun, Y. Yu, S. Dong, K. Wang, and J. Yang. 2021. Optimal Scheduling Considering Different Energy Hub Model of Integrated Energy System. Proceedings of the 2021 IEEE 4th International Conference on Renewable Energy and Power Engineering (REPE). Beijing, China, 9-11 October. IEEE Publisher.

[16] M. S. Javadi, A. Anvari-Moghaddam, and J. M. Guerrero. 2017. Optimal scheduling of a multi-carrier energy hub supplemented by battery energy storage systems. Proceedings of the 2017 IEEE International Conference on Environment and Electrical Engineering and 2017 IEEE Industrial and Commercial Power Systems Europe (EEEIC / I&CPS Europe). Milan, Italy, 6-9 June. IEEE Publisher.

[17] W. Geng and L. Jia. 2020. Hybrid Genetic Particle Swarm Optimization Based Economical Operation of Energy Hub. Proceedings of the 2020 5th International Conference on Power and Renewable Energy (ICPRE). Shanghai, China, 12-14 September. IEEE Publisher.

[18] L. Wang. 2023. Optimal Scheduling Strategy for Multi-Energy Microgrid Considering Integrated Demand Response. Energies 16(12): 4694.

[19] C. Timothée; A. T. D. Perera; J.-L. Scartezzini; and D. Mauree. 2017. Optimum dispatch of a multi storage and multi-energy hub with demand response and restricted grid interactions. Energy Procedia 142: 2864-2869.

[20] Y. G. Son; B. C. Oh; M. A. Acquah; R. Fan; D. M. Kim; and S. Y. Kim. 2021. Multi Energy System With an Associated Energy Hub: A Review. IEEE Access 9: 127753 – 127766.

[21] A. Shammary, A. A. Hafez, A. F. M. Ali, A. A. Mahmoud, M. I. Mohamed, and M. A. Merazy. 2022. Energy Hub Modeling and Operation, A Comprehensive Review. Proceedings of the 2022 23rd International Middle East Power Systems Conference (MEPCON). Cairo, Egypt, 13-15 December. IEEE Publisher.

[22] A. Maroufmashat; S. T. Taqvi; A. Miragha; M. Fowler; and A. Elkamel. 2019. Modeling and Optimization of Energy Hubs: A Comprehensive Review. Inventions 4(3): 50.

[23] T. Ding; W. Jia; M. Shahidehpour; O. Han; Y. Sun; and Z. Zhang. 2022. Review of Optimization Methods for Energy Hub Planning, Operation, Trading, and Control. IEEE Transactions on Sustainable Energy 13(3): 1802-1818.

[24] S. H. R. Hosseini; A. Allahham; S. L. Walker; and P. Taylor. 2020. Optimal planning and operation of multi-vector energy networks: A systematic review. Renewable and Sustainable Energy Reviews 133: 110216

[25] K. Rojanaworahiran and K. Chayakulkheeree. 2021. Probabilistic Optimal Power Flow Considering Load and Solar Power Uncertainties Using Particle Swarm Optimization. GMSARN International Journal 15(1): 37-43.

[26] J. Manwell; J. McGowan; and A. L. Rogers. 2002. Wind Energy Explained: Theory, Design and Application. Chichester: John Wiley & Sons.

[27] S. Dechjinda and K. Chayakulkheeree. 2024. Optimal Daily Scheduling of Hybrid Wind-Hydrogen Storage using Particle Swarm Optimization. Proceedings of the 2024 12th International Electrical Engineering Congress (iEECON). Pattaya, Thailand, 6-8 March. IEEE Publisher.

[28] C. Yammani; S. Maheswarapu; and M. Kumari. 2012. Optimal Placement of Multi DGs in Distribution System with Considering the DG Bus Available Limits. Energy and Power 2(1): 18-23.

[29] S. Ould Amrouche; D. Rekioua; T. Rekioua; and S. Bacha. 2016. Overview of energy storage in renewable energy systems. International Journal of Hydrogen Energy 41(45): 20914-20927.

[30] G. Cau; D. Cocco; M. Petrollese; S. Knudsen Kær; and C. Milan. 2014. Energy management strategy based on short-term generation scheduling for a renewable microgrid using a hydrogen storage system. Energy Conversion and Management 87: 820-831.

[31] J. Kennedy and R. Eberhart. 1995. Particle swarm optimization. Proceedings of the ICNN'95 - International Conference on Neural Networks. Perth, WA, Australia, 27 November – 1 December. IEEE Publisher.

[32] P. Muangkhiew and K. Chayakulkheeree. 2024. Probabilistic Fuzzy Multi-Objective Optimal Power Flow. GMSARN International Journal 18(2): 213-222.

[33] H. K. Anna Sandhaas, César De Jesús, and Niklas Hartmann. 2022. Generation of Industrial Electricity and Heat Demand Profiles for Energy System Analysis. Proceedings of the IAEE International Conference.

[34] W. Piawises and K. Chayakulkheeree. 2024. Smart Home Energy Management Algorithm for TOU Based Demand Response. Proceedings of the 2024 12th International Electrical Engineering Congress (iEECON). Pattaya, Thailand, 6-8 March. IEEE Publisher.